Correspondence: Dr. Alan M. Jones
Address: Department of Biology
The University of North Carolina at Chapel Hill
Coker Hall, CB#3280

Phone : (919) 962-6932
Fax: (919) 962-1625
E-mail: alan_jones@unc.edu

The author responsible for distribution of materials integral to the findings presented in this article is Dr. Alan Jones alan_jones@unc.edu

Running Title: Biased System Signaling

26 **Title: Biased Signaling: Distinct Ligand-directed Plasma Membrane**

27 **Signalosomes Using a Common RGS/ G protein Core**

28 **AUTHORS Timothy J. Ross-Elliott[1], Justin Watkins[1], Xiaoyi Shan[2], Fei Lou[1], Bernd**

29 **Dreyer[1], Meral Tunc-Ozdemir[1], Haiyan Jia[1], Jing Yang[1], Luguang Wu[2], Yuri Trusov[3],**

30 **Patrick Krysan[4], and Alan M. Jones[1, 3, 5]**

31 Department of [1] Biology and [3] Pharmacology, University of North Carolina at Chapel Hill, Chapel

32 Hill, NC 27599, USA.

33 [2]Beijing Forestry University, Beijing China 1000083

34 [3]School of Agriculture and Food Science, The University of Queensland, St. Lucia, Q4072,

35 Australia.

36 [4]Department of Horticulture, University of Wisconsin Madison, Madison, WI 53706, USA

37 [5]Lead Contact

38 *Correspondence: alan_jones@unc.edu

39

40 **Keywords:** Arrestin analog, AtRGS1, calcium signaling, clathrin-mediated endocytosis, MAPK
41 activation, proximity labeling, sterol-dependent endocytosis, VPS26, WNK kinase,

42

43 **Abbreviations: *Arabidopsis thaliana* Regulator of G Signaling (AtRGS1), Clathrin-Mediated**
44 **Endocytosis (CME), Sterol-Dependent Endocytosis (SDE), Total Internal Reflection**
45 **Fluorescence Microscopy (TIRF), Clathrin Light Chain (CLC), Flotilin 1 (FLOT1),**
46 **Vacuolar Protein Sorting 26 (VPS26)**

SUMMARY

Biased signaling occurs when different ligands that are directed at the same receptor launch different cellular outcomes. Because of their pharmacological importance, we know the most about biased ligands and little is known about other mechanisms to achieve signaling bias. In the canonical animal G protein system, endocytosis of a 7-transmembrane GPCR desensitizes a cell from its extracellular signal. β-arrestins facilitate GPCR endocytosis but also propagate cytoplasmic signaling depending on the bias. In Arabidopsis, GPCRs are not required for G protein coupled signaling because the heterotrimeric G protein complex spontaneously exchanges nucleotide. Instead, the prototype 7-transmembrane Regulator of G Signaling 1 protein AtRGS1 modulates G signaling and through ligand-dependent endocytosis, de-repression of signaling is initiated but canonical arrestins are not involved. Endocytosis initiates from two separate pools of plasma membrane: microdomains and a clathrin-accessible neighborhood, each with a select set of discriminators, activators, and newly-discovered arrestin-like adaptors. Different trafficking origins and trajectories lead to different cellular outcomes. Thus, compartmentation with its attendant signalosome architecture is a previously unknown mechanism to drive biased signaling.

INTRODUCTION

Different ligands discriminated by the same receptor or utilizing the same core of signaling elements can set in motion a cascade of events that lead to multiple outcomes. When subsets of outcomes are ligand-specific, we label this biased signaling. This bias can be encoded in the ligand structure (biased ligands), in the receptors (biased receptors), or in the interactions between the signaling components (biased systems) (Smith et al., 2018). Of the three defined mechanisms,

70 biased ligands is the most widely studied because of its immediate pharmacological significance,
71 such as the development of drugs that provide analgesia without the addictive side effect (Manglik
72 et al., 2016; White et al., 2015; Wingler et al., 2019). **a)** Ligand bias occurs when a ligand stabilizes
73 one or few of several conformations of a receptor protein which then preferentially recruits or
74 activates signaling elements such as arrestin and the heterotrimeric G protein complex that lead
75 toward one cellular outcome over another (Bohn et al., 2000; DeWire et al., 2013). For example,
76 some ligands are biased towards β-arrestins (aka arrestin-2 and -3) signaling (Charest et al., 2007;
77 Gesty-Palmer et al., 2006; Shenoy et al., 2006) such as certain dopamine agonists compared to
78 dopamine which is biased towards D_2R-β-arrestin coupling (Allen et al., 2011). Certain opioid
79 agonists compared to morphine are biased toward G-protein signaling (DeWire et al., 2013; Rives
80 et al., 2012; White et al., 2015). **b)** Receptor bias occurs through recognition of the same ligand
81 by multiple receptor types (Géhin et al., 1999) including so-called decoy receptors (Lin and Hsieh,
82 2011; Pan et al., 1997), some of which may in fact be functional receptors that use non-classical
83 signaling pathways (Lin and Hsieh, 2011; Rajagopal et al., 2010a). Dopamine D_1 and D_2 class
84 receptors recognize dopamine, but signal through different subunits of Gα as well as arrestin (Urs
85 et al., 2017). **c)** System bias involves a cell-mediated shift to one pathway over another by some
86 unknown mechanism but one possibility is through mass action, for example, making arrestin more
87 abundant at the receptor than Gα or a particular kinase (Urs et al., 2016). This last category of bias
88 signaling is the least understood and the subject of the present work.

89 Phosphorylation patterns are the chemical bar codes for biased signaling at least for
90 arrestin-dependent outcomes (Butcher et al., 2011; Nobles et al., 2011; Shiraishi et al., 2018; Yang
91 et al., 2015; Yang et al., 2017). G-protein coupled Receptor Kinases (GRKs) phosphorylate the C-
92 terminus or other cytoplasmic elements of GPCRs in response to agonist binding (Choi et al.,

93 2018), unlike Protein Kinase A and C that phosphorylate GPCRs in a heterologous manner
94 (Benovic et al., 1986; Sibley et al., 1987). The subsequent coupling of arrestin to phosphorylated
95 GPCRs does not end G-protein-independent signaling. Arrestin-bound GPCRs further activates
96 some multiple kinase pathways including MAPK and tyrosine kinases (DeFea et al., 2000; Luttrell
97 et al., 2001; Rajagopal et al., 2010b) but not all (e.g. (O'Hayre et al., 2017)). While plants lack
98 GRKs, an Arabidopsis family of kinases called WITH NO LYSINE (**WNK**) Kinase phosphorylate
99 the C-terminal tail of the non-canonical 7-transmembrane Regulator of G Signaling (**AtRGS1**) in
100 response to extracellular glucose (Fu et al., 2014; Urano et al., 2012). AtRGS1 is also
101 phosphorylated by other kinases including BAK1, a co-receptor for flg22 which is a Pathogen-
102 Associated Molecular Pattern (PAMP) (Liang et al., 2018; Tunc-Ozdemir et al., 2017; Tunc-
103 Ozdemir et al., 2016) and loss of AtRGS1 and other G protein components severely affect
104 resistance in a wide range of pathogens (Zhong et al., 2018). System-biased signaling may be
105 particularly relevant in plants where AtRGS1 modulates intracellular signaling transduction
106 through G protein activation. AtRGS1 regulates G protein activation with ligand discrimination
107 likely facilitated by membrane bound Receptor Like Kinases (RLKs) of which there are more than
108 600 members in Arabidopsis (Shiu and Bleecker, 2001).

109 In animals, activation of G Protein signaling results from GDP exchange for GTP on the
110 Gα subunit, wherein this nucleotide exchange is the rate-limiting step (Ferguson et al., 1986).
111 Desensitization of the cell toward the signal occurs through endocytosis of the GPCR mediated by
112 arrestins (Benovic et al., 1987; Lohse et al., 1990). In Arabidopsis, however, the Gα subunit,
113 AtGPA1, spontaneously exchanges nucleotides without a GPCR thus it is self-activating with the
114 intrinsic GTPase activity being the rate-limiting step (Johnston et al., 2007; Jones et al., 2011a).
115 AtRGS1 accelerates the intrinsic GTPase of AtGPA1 (Jones et al., 2011b) and as a result, inactive

116 Gα remains bound to GDP until de-repression through AtRGS1 endocytosis, permitting Gα
117 activation through nucleotide exchange and subsequent downstream signal transduction (Urano et
118 al., 2012). This AtRGS1 endocytosis is a well-established proxy for sustained G protein activation
119 and the proportion of endocytosed AtRGS1 is linearly related to the proportion of G protein
120 activation (Fu et al., 2014). In Arabidopsis, sugars (Fu et al., 2014; Grigston et al., 2008) and flg22
121 (Tunc-Ozdemir et al., 2016) activate AtRGS1 (Urano et al., 2012).

122 Physically de-coupling AtRGS1 from the heterotrimeric G protein complex by endocytosis
123 is the engine of the de-repression mechanism, at least for sustained activation. There are two modes
124 of endocytosis in plants: Clathrin-Mediated Endocytosis (**CME**) and Sterol-Dependent
125 Endocytosis (**SDE**) (Fan et al., 2015), however, the protein that directly couples to AtRGS1 and is
126 responsible for endocytosis is unknown. Extensive work elucidated the CME pathway in animal
127 and yeast systems with the function of many molecular components being well characterized. Of
128 particular interest is the ADAPTOR PROTEIN COMPLEX-2 (**AP-2**) that is required for
129 recognition and binding of cargo (Jackson et al., 2010; Kelly et al., 2008; Krauss et al., 2006),
130 recruiting clathrin to the PM, and the subsequent formation of clathrin-coated vesicles. In the
131 absence of AP-2 function, clathrin-coated vesicle formation is reduced and endocytosis is inhibited
132 (Boucrot et al., 2010). The AP-2 complex is a heteromeric complex consisting of 2 large subunits
133 (α2 and β2), 1 medium subunit (μ2), and 1 small subunit (σ2) (Collins et al., 2002).

134 SDE is a clathrin-independent mechanism for internalization of membrane-associated
135 proteins. Sometimes referred to as lipid raft endocytosis, SDE of these microdomains requires
136 flotilin1 (**Flot1**), and possibly the microdomain-associated remorin protein (Raffaele et al., 2009)
137 for internalization of sterol-rich vesicles (Li et al., 2012). Membrane proteins PIP2;1 and

138 Respiratory Burst Oxidase Homolog D (**RbohD**) are selectively internalized via sterol-dependent
139 endocytosis under salt stress conditions (Hao et al., 2014; Li et al., 2011).

140 We present data illustrating a biased system where two distinct extracellular ligands induce
141 endocytosis of AtRGS1 from separate plasma membrane origins, of which one is mediated by a
142 an arrestin-fold-containing protein, Vacuolar Protein Sorting 26 (VPS26). flg22 initiates AtRGS1
143 endocytosis via CME, while glucose activates both pathways of endocytosis. Phosphorylation of
144 AtRGS1 and involvement of individual subunits of the heterotrimeric G protein complex are also
145 ligand specific as are the immediate downstream consequences. From the CME-mediated-
146 AtRGS1 origin, flg22 induces a MAPK cascade known to drive transcriptional reprogramming
147 (Lee et al., 2015), whereas from the SDE-mediated-AtRGS1 origin, glucose induces
148 transcriptional change that is independent of the MAPK cascade.

149 **RESULTS**

150 **Biased Signaling by Two Extracellular Signals**

151 To date, there are 2 well-studied signals that directly and rapidly activate the Arabidopsis
152 heterotrimeric G protein signaling pathway through AtRGS1 endocytosis: **1)** flg22 which is a 22-
153 amino acid PAMP from the plant pathogen *Pseudomonas syringe* that is recognized on plant cells
154 to initiate the innate immunity pathway (Asai et al., 2002; Felix et al., 1999; Gómez-Gómez and
155 Boller, 2000). It is already established that flg22 is perceived extracellularly (e.g. (Jelenska et al.,
156 2017) by co-receptors BAK1 and FLS2 as part of a larger G protein complex (Sun et al., 2013;
157 Tunc-Ozdemir and Jones, 2017). **2)**. Glucose or a glucose metabolite which are products of
158 photosynthesis (Tunc-Ozdemir et al., 2018) and metabolism of starch stores (Pharr and Keller,
159 2017).

160 Many sugars, although primarily sucrose, are transported extracellularly in the apoplastic
161 space where they are converted to glucose by cell wall localized invertases and potentially further
162 metabolized to a signal. These sugars are rapidly taken up through a large family of transporters
163 (Chen et al., 2010; Williams et al., 2000) where they are detected in the cytoplasm, but some sugars
164 may also be detected extracellularly (Li and Sheen, 2016). D-glucose or its metabolite induces
165 rapid endocytosis of AtRGS1-dependent sugar signaling (Fu et al., 2014; Urano et al., 2012) and
166 because AtRGS1 shares the membrane topology of GPCRs which perceive extracellular signals,
167 it has been assumed that the extracellular glucose or metabolite is perceived by the AtRGS1/G
168 protein complex. However, neither an extracellular site for perception nor direct evidence for
169 agonist binding to AtRGS1 has been shown. To address the former, impermeant sugars were
170 tested for the ability to activate G signaling.

171 The glucose-fructose dissacharide 6-0-α-D-glucopyranosyl-D-fructose (aka isomaltulose,
172 pallatinose), is presumed not to be transported across the plant cell membrane although it acts as
173 an active glucose precursor if synthesized intracellularly (Loreti et al., 2000; Sinha et al., 2002).
174 While the expression of sucrose isomerase in potato increased apoplastic isomaltulose, transport
175 across any membrane has yet to be demonstrated (Börnke et al., 2002). Importantly, isomaltulose
176 is not hydrolyzed extracellularly (Fernie et al., 2001; Wu and Birch, 2011). To determine if
177 isomaltulose is impermeant to the plasma membrane, we chemically synthesized [^{14}C]
178 isomaltulose (Figure S1A) and tested for uptake into Arabidopsis seedlings. Isomaltulose was at
179 least 9-fold less permeant to cells than glucose (Figure S1B). Therefore, to determine if sugars are
180 perceived extracellularly by hypocotyl cells, we tested the effect of isomaltulose on AtRGS1-YFP
181 endocytosis (Figure 1A) as a validated proxy for activation of G signaling as previously shown
182 (Fu et al., 2014; Urano et al., 2012). Whereas several mono and disaccharides failed to activate G

183 signaling, extracellular isomaltulose caused AtRGS1 internalization more effectively ($P < 0.01$)
184 than D-glucose (Figure 1B) despite being transported ~10-fold less suggesting that isomaltulose
185 activates AtRGS1 extracellularly. The 5% D-glucose impurity in the isomaltulose preparation
186 would induce at most 5% AtRGS1 internalization and therefore does not account for the observed
187 level of activation. Turanose is another disaccharide that is thought to be perceived extracellularly
188 (Loreti et al., 2000) and is impermeant (Rolland et al., 2002) therefore endpoint analysis was
189 performed using this sugar, and just as for both glucose and isomaltulose, turanose activated G
190 signaling (Figure 1C). Isomaltulose and turanose are disaccharides that share a glucose ring
191 (Figure 1D), suggesting that glucose or a glucose metabolite is the discriminated signal or is
192 important for a metabolic agonist (e.g. sugar nucleotides).

193 **AtRGS1 Endocytic Pathway is Signal Biased**

194 Having shown that extracellular flg22 is detected by BAK1/FLS2 (Chinchilla et al., 2006; Gómez-
195 Gómez and Boller, 2000; Tunc-Ozdemir et al., 2016) and induces AtRGS1 endocytosis (Tunc-
196 Ozdemir et al., 2016) and that extracellular D-glucose acts upstream of AtRGS1 endocytosis, both
197 requiring at least in part the phosphorylation of AtRGS1 at its C terminal tail (Tunc-Ozdemir et
198 al., 2016; Urano et al., 2012), we turned to the question of whether these two signals activate the
199 same pool of AtRGS1. Endocytosis in plants utilizes two primary pathways: CME and SDE. Both
200 pathways have been individually associated with the activity of specific proteins and responses
201 (Adam et al., 2012; Dhonukshe et al., 2007; Irani et al., 2012; Li et al., 2012); for example, CME
202 and SDE cooperatively regulate the activity of RbohD in the flg22 pathway (Hao et al., 2014). We
203 used high-resolution microscopies to achieve the needed spatial and temporal resolution to answer
204 quantitative differences in signal-induced activation. To determine if one or both pathways
205 regulate AtRGS1 activity at the membrane, we induced internalization with D-glucose and *flg22*

206 while simultaneously inhibiting the CME pathway by arresting AP2μ function with
207 TyrphostinA23 (**TyrA23**) (Banbury et al., 2003; Dhonukshe et al., 2007) or inhibiting the SDE
208 pathway by suppressing microdomain formation via sterol solubilization with methyl-β-
209 cyclodextrin (**MβCD**) (Ilangumaran and Hoessli, 1998; Ohtani et al., 1989). MβCD, even at great
210 excess, did not block *flg22*–induced AtRGS1 internalization compared to the control ($p<0.01$)
211 (Figure 2A). Conversely, AtRGS1 internalization induced with glucose was reduced nearly 50%
212 compared to baseline with a minimum concentration of 5mM MβCD (Figure 2B). This suggests
213 that roughly half of the D-glucose-regulated pool of AtRGS1 is located in a SDE domain. To
214 determine if the CME pathway regulates AtRGS1 activity, we applied TyrA23 with *flg22* or D-
215 glucose. AtRGS1 internalization with both activators was significantly reduced ($p<0.01$);
216 completely for flg22-induced AtRGS1 endocytosis (Figure 2C) and by 50% for D-glucose-induced
217 AtRGS1 endocytosis (Figure 2D). The structurally similar but inactive TyrA23 analog
218 TyrphostinA51 showed no significant effect on AtRGS1 internalization ($p<0.01$) (Figure 2C and
219 2D, TyrA51), indicating that the inhibitory effect of TyrA23 is chemically specific (Banbury et
220 al., 2003). When both inhibitors were applied simultaneously with glucose, AtRGS1
221 internalization was ablated (Figure 2E). These results suggest that there is a single flg22-induced
222 pool that internalizes through a CME pathway and that there are two distinct glucose-induced
223 pools, one internalizes through the CME pathway and the other through the SDE pathway. Because
224 the glucose-induced pool is equally inhibited by the CME and SDE inhibitors, a rapid equilibrium
225 between the pools is not likely, otherwise neither inhibitor would have shown efficacy.

226 To further test our hypothesis of ligand-dependent membrane origins of AtRGS1
227 endocytosis, we used a genetic approach by measuring AtRGS1 internalization in the AP-2μ null
228 mutant, *ap2m* (Kim et al., 2013). The AP-2 complex plays a critical role in transporting cargo in

229 the CME pathway, whereby the μ subunit of this tetrameric AP-2 complex directly interacts with
230 cargo proteins during endocytosis (Bashline et al., 2013; Krauss et al., 2006). In the *ap2m* mutant
231 seedlings, flg22-induced AtRGS1 internalization was ablated ($p<0.01$), consistent with the
232 TyrA23 results (Figure 2F). In contrast, glucose resulted in less AtRGS1 internalization in the
233 *ap2m* mutant compared to Col-0 wild type ($p<0.01$). The addition of MβCD with glucose ablated
234 AtRGS1 internalization in the *ap2m* mutant to basal levels (Figure 2G). These observations are
235 consistent with two signal-dependent pools of AtRGS1 on the plasma membrane; 1) a homogenous
236 pool for flg22 signaling and 2) a conglomerate pool for D-glucose signaling.

237 **A Point Mutation in the 7 Transmembrane Domain Disarms Biased Signaling**

238 The μ subunit of the AP-2 complex is a cargo recognition and interaction component in the CME
239 pathway. It binds to known tyrosine motifs, YXXΦ, where X is any amino acid and Φ is an amino
240 acid with a hydrophobic side chain (Ohno et al., 1995). The second cytoplasmic loop in AtRGS1
241 contains such a motif with the amino acid sequence Y^{112}FIF (Chen et al., 2003). To determine if
242 this motif is necessary for AtRGS1 endocytosis and a potential binding motif for AP-2μ, we
243 generated AtRGS1 with a tyrosine to alanine mutation ($AtRGS1^{Y112A}$). flg22 failed to induce
244 endocytosis of the $AtRGS1^{Y112A}$ mutant (Figure 2H). Glucose-induced internalization of the
245 $AtRGS1^{Y112A}$ was reduced to half ($p<0.05$) compared to wild type internalization and was further
246 reduced to the resting level with the addition of MβCD ($p<0.01$) (Figure 2I) demonstrating that
247 the Y^{112}FIF is necessary for internalization and likely a recognition and binding site for AP-2μ.
248 The flg22-induced AtRGS1 pool is entirely mediated by the CME pathway whereas roughly half
249 of the D-glucose-induced AtRGS1 pool internalizes through the CME pathway.
250

251 **Physically-Distinct, Dynamic Populations of AtRGS1: Architectural Basis for Biased**
252 **Signaling**

253 We showed through pharmacological and genetics approaches that two signal-dependent pools of
254 AtRGS1 exist raising the possibility that the two AtRGS1 pools are physically distinct on the cell
255 membrane. The differential dependence on sterol and clathrin for partial glucose- vs. flg22-
256 induced endocytosis of AtRGS1 suggests this is the case. To test this hypothesis, we imaged
257 AtRGS1 with a GFP C-terminal tag using Total Internal Reflection Microscopy (**TIRF**) and
258 IMARIS (v9.2.2, Bitplane Inc) surface tracking (Figure S2 A-E, examples of raw data). We
259 calculated the average size and speed of AtRGS1 proteins during a 30-second interval taken from
260 time-lapse imaging at 5 and at 15 minutes post treatment with glucose and flg22. Two clearly
261 distinct signal-dependent populations of AtRGS1 were observed (Figure 2J). After 5 minutes under
262 glucose conditions, the surface area of AtRGS1-GFP clusters were significantly larger ($\ddot{x}$ = 0.9403
263 μm^2 n=4619) than flg22 at ($\ddot{x}$ = 0.5998 μm^2 n=2026) (Figure 2J inset) ($p<0.01$). At 15 minutes,
264 the area of flg22 treated AtRGS1-GFP increased slightly to 0.6733 μm^2 (n=1751), with glucose
265 treated AtRGS1-GFP, the area increased to 1.0072 μm^2 (n=6209) (Figure S2 F-H). Velocity
266 differences for AtRGS1-GFP remain consistent between 5 and 15 minutes with flg22-treated
267 AtRGS1 averages at 1.53µm/s and 1.63µm/s, respectively (n= 2026 and 1751) and glucose-treated
268 AtRGS1 averages at 0.98µm/s and 1.01µm/s at 5 and 15 minutes, respectively (n= 4619 and 6209).
269 Two populations of differently sized AtRGS1 protein clusters provides structural support for two
270 origins of endocytosis.

271 **The Signal Dependency Correlates with Endocytosis Marker Redistribution**

272 The Clathrin Light Chain (**CLC**) and Flot1 proteins are associated with CME and SDE,
273 respectively (Fan et al., 2015; Li et al., 2012). We generated transgenic lines expressing AtRGS1-

274 GFP with either CLC-mCherry or Flot1-mCherry endocytosis markers to investigate the
275 localization of AtRGS1 in relation to both markers. We imaged the response of both endocytosis
276 markers 5 minutes after application of water, flg22, and glucose to look for changes in marker
277 distribution in the cell (Figure 2K-P). Using Manders Overlap Coefficient, we quantified the co-
278 occurrence of both endocytosis markers with AtRGS1-GFP under all treatment conditions. We are
279 using Manders instead of Pearson's Correlation because our qualitative analysis shows a ligand
280 dependent change in marker localization and shape. We simply want to quantify the change in
281 overlap of the two signals (Manders) and not the change in signal intensity (Pearsons) that may
282 simply be a result of AtRGS1 internalization and not correlated to direct interaction with either
283 endocytosis marker.

284 A subset of the Manders Overlap Coefficients after background subtraction are shown in
285 Figure 2Q-V and correspond to the confocal micrographs in Figure 2K-P. M1 represents the
286 proportion of total GFP that overlaps with mCherry. Similarly, M2 represents the proportion of
287 total mCherry for CLC or FLOT1 that overlaps with GFP. Under conditions with no signaling
288 ligand (Figure 2K and 2N), RGS1-GFP and our endocytosis markers have a high overlap baseline
289 (Figure 2Q and 2R). Due to the restrictive cytoplasmic space, we believe this is not functional
290 interaction, merely fluorescence overlap due to high protein crowding and resolution limitation.
291 After flg22 addition (Figure 2L and 2O), the proportion of CLC associated with RGS1 decreased,
292 with the proportion of RGS1 overlapping with CLC also decreasing significantly ($p<0.01$) (Figure
293 2S. Simply stated, a smaller defined subset of the RGS1 and CLC populations are overlapping
294 with each other in a ligand-dependent manner with the endocytosis marker also exhibiting a
295 structural change. This response was not observed with FLOT1 when flg22 was added (Figure
296 2T). With glucose addition (Figure 2M and 2P) CLC showed no significant change compared to

297 water (Figure 2U), while FLOT1 overlap decreased with RGS1 compared to the water baseline
298 ($p<0.01$) (Figure 2V). The same responses were observed at 15 minutes post ligand addition
299 (Figure S2 I-T). The averages for the entire collection of M2 scores from all samples are presented
300 in Figure 2W. These results indicate that endocytosis markers are responding to specific ligands
301 and subsets of the total marker and AtRGS1 protein populations are overlapping in a signal specific
302 manner. In summary, the different intrinsic trafficking properties further support at least two pools
303 of ligand-activated AtRGS1.

304 **Signaling Bias Involves Phosphorylation from Different Kinases.**

305 Phosphorylation of AtRGS1 is a necessary requisite for both glucose- and flg22-induced
306 endocytosis. The C-terminus of AtRGS1 contains multiple di-serine residues that could function
307 as potential phosphorylation sites for signal transduction. A truncated version of AtRGS1 lacking
308 the 43 most C-terminal residues, AtRGS1$^{\Delta Ct}$, served as a blunt phosphorylation-deficient mutation
309 to determine if the C-terminal tail, in particular any C-terminal serines located there are necessary
310 for AtRGS1 endocytosis (Figure S4A). Application of flg22 failed to internalize the AtRGS1$^{\Delta Ct}$
311 mutant compared to water control ($p<0.01$) (Figure 3A). Glucose application however, internalized
312 the AtRGS1$^{\Delta Ct}$ mutant, but at 50% the level of the wild type AtRGS1 ($p<0.01$). MβCD completely
313 inhibited internalization of the AtRGS1$^{\Delta Ct}$ mutant levels ($p<0.01$) (Figure 3B). These results show
314 that the C-terminus is necessary for flg22- and glucose-induced endocytosis of AtRGS1 and
315 support two subpopulations of AtRGS1 among the glucose-induced pool.

316 Three phosphorylated serine residues on the C-terminus of AtRGS1 at positions 428, 435,
317 and 436 are necessary for at least partial endocytosis of AtRGS1 induced by both glucose and
318 flg22. Therefore, we mutated these serines to alanine (AtRGS1^{3SA}) to determine if those specific
319 residues were necessary to induce internalization by either agonist. Upon treatment with flg22,

320 AtRGS1^{3SA} internalization was at basal levels compared to wild type ($p<0.01$) (Figure 3C),
321 confirming previous results by Tunc-Ozdemir *et al* (Tunc-Ozdemir et al., 2016) and suggesting
322 that the CME pathway is dependent on phosphorylation of serines 428, 435 and/or 436. In the case
323 of glucose, endocytosis was only partially impaired by the AtRGS1^{3SA} mutant ($p<0.01$) (Figure
324 3D). MβCD completely blocked glucose-induced endocytosis of the AtRGS1^{3SA} mutant (Figure
325 3D), consistent with our previous results that show glucose-induced internalization utilizes both
326 CME and SDE pathways and that the CME pathway requires phosphorylation at $Ser_{428/435/436}$.
327 These results enable us to exclude an osmotic effect that effectively sequesters a portion of
328 the plasma membrane pool of AtRGS1 into a sterol-dependent, or at least an MβCD-inhibitable,
329 microdomain that is incapable of internalizing its components. If an osmotic effect occurred, the
330 presence of MβCD would have prevented formation of these microdomains and consequently the
331 sequestration of AtRGS1 for the endocytic pool would cause 100% internalization by glucose.
332 This was not observed.

333 **System Bias by Skewed Kinase and G-protein Complex Composition**

334 Because the cluster of phosphorylated serines on the C-terminus of AtRGS1 are required for
335 AtRGS1 internalization, we hypothesize that one mechanism for system bias is to functionally-
336 sequester cognate kinases for glucose and flg22 in their respective ligand-delineated pools. To test
337 this hypothesis, we quantified AtRGS1 internalization in the mutant backgrounds of the flg22-
338 activated FLS2 kinase (*fls2*) and BAK1 co-receptor (*bak1*) and the D-glucose-activated WNK
339 kinase (*wnk8*-2, *wnk1*-1) null mutants. Upon treatment with flg22, AtRGS1 endocytosis was
340 ablated in *fls2* and *bak1-4* mutants ($P<0.01$), while glucose-induced internalization in these
341 mutants was unaffected ($P=0.70$ and 0.37 respectively) (Figure 3E and 3F). In contrast, D-glucose-
342 induced internalization in the *wnk8-2* was ablated ($p<0.01$), while flg22-induced AtRGS1

343 endocytosis was unaffected (P=0.89) (Figure 3G). Interestingly, a low dose, long duration
344 application of 2% glucose over 6 hours to *wnk1-1* had no discernable affect compared to wild type
345 (Figure S3A), prompting a revisit of the proposed mechanism that WNK1 kinase mediates low
346 dose-long duration activation by glucose (Fu et al., 2014). Our results suggest that FLS2 and
347 BAK1 are specific to the CME pathway and WNK8 kinase is specific to the SDE pathway.

348 The canonical components of the heterotrimeric G protein complex are necessary for
349 glucose-induced internalization of AtRGS1 (Fu et al., 2014; Urano et al., 2012). More specifically,
350 Gβγ is required for the recruitment of WNK kinases for phosphorylation of AtRGS1, leading to
351 AtRGS1 endocytosis and activation of downstream G signaling. We hypothesized that individual
352 components of the G protein heterotimer may be required for biased signaling. To test this
353 hypothesis, we quantified AtRGS1 endocytosis in G protein mutant backgrounds after flg22 and
354 glucose activation. In the AtGPA1 (Gα) null background, *gpa1-4,* AtRGS1 endocytosis showed
355 no significant difference compared to wild type when glucose was applied (p=0.48) (Figure 3H).
356 After addition of flg22, however, AtRGS1 endocytosis was at basal levels ($p < 0.01$) in the absence
357 of Gα indicating that the G subunit is essential for this pathway (Figure 3H). We additionally tested
358 AtRGS1 in the absence of XLG2, one member of a three-gene family of atypical, G proteins. XLG
359 proteins have a homologous C-terminal Gα domain and N-terminal nuclear localization signal
360 (Ding et al., 2008). Loss of XLG2 in the *xlg2-1* mutant, did not affect AtRGS1 endocytosis by
361 glucose application (p=0.43), but completely inhibited AtRGS1 endocytosis to basal levels after
362 addition of flg22 ($p<0.01$) (Figure 3I). Additionally, low dose, long duration glucose application
363 had no effect in the *xlg2*-1 mutant compared to wild type (Figure S3B). In the *agb1-2/agg1* double
364 null mutant, AtRGS1 endocytosis was diminished after addition of flg22 ($p<0.01$) (Figure 3J).
365 Loss of the Gβγ dimer in the *agb1-2/agg1* mutant had no effect on glucose-induced AtRGS1

366 endocytosis compared to wild type after 30 minutes of treatment with 6% D-glucose (p=0.79)
367 (Figure 3J). Interestingly, a 2% - 6 hour application of D-glucose required AGB1/AGG1 for
368 activation (p<0.01) (Figure 3K).

369 **VPS26 a Candidate Plant β-arrestin-like Adaptor Necessary for AtRGS1 Endocytosis in the**
370 **CME Pathway: Discovery and Validation**

371 In the animal G signaling pathway, GPCR endocytosis results in β–arrestin-mediated
372 desensitization of the cell from an extracellular signal. Higher plant genomes do not encode
373 ancestral α-arrestins or canonical (i.e. visual and nonvisual) arrestins (Alvarez, 2008). We sought
374 candidate adaptors for AtRGS1 that may function like β-arrestins to recruit AP2/clathrin to
375 AtRGS1 for endocytosis by querying 3-D structure databases. As shown in Figure S4A and B, we
376 identified three *Arabidopsis* VACUOLAR PROTEIN SORTING 26 (VPS26) proteins that contain
377 arrestin folds (Oliviusson et al., 2006) and are orthologous to human VPS26. *Arabidopsis* VPS26A
378 and VPS26B amino acid sequences are 91% identical whereas VPS26-like is 20% identical to
379 VPS26A and VPS26B. In mammals and plants, VPS26 operates with VPS29 and VPS35 in the
380 retromer complex on the endosome (Zelazny et al., 2013). This raises the possibility that VPS26
381 proteins have a moonlighting function in modulating AtRGS1 internalization.

382 To compare the arrestin and AtVPS26A protein structures, we first created a model of
383 AtVPS26A using MODELLER (Martí-Renom et al., 2000). Toward this, a high quality
384 homogeneous sequence alignment was generated using the VPS26 family (Arabidopsis VPS26A,
385 VPS26B, VPS26like and Homo sapiens VPS26A) and arrestin family (Vertebrates: Human
386 arrestin-1 and arrestin-2; bovine arrestin-1, arrestin-2, arrestin-2, and a variant p44; Squid arrestin-
387 1; and the invertebrate shrimp arrestin (Figure S5A). Human, bovine, and squid sequences were
388 included because PDB structures are available. The squid and shrimp sequences were added for

389 divergence information (among the opistokonts). AtVPS26A and human VPS26A share 56.48%
390 sequence identity while AtVPS26A and arrestins share only 14-17% sequence identities (Figure
391 S5B). These results rationalized our use of the high-resolution (2.1Å) crystal structure of *Homo*
392 *sapiens* Vps26a (PDB [2FAU]) rather than an arrestin structure to generate models of AtVPS26A
393 for subsequent comparison to arrestin. Details of the top five selected models (atvps26a1 →5) are
394 provided in the Methods.

395 We compared the atvps26a-2 model with the bovine arrestin-3 (PDB [3P2D (Zhan et al.,
396 2011)]). Although the primary amino acid identity between arrestin and AtVPS26A is only ~15%
397 (Figure 4A), the structure of AtVPS26A model shows a remarkably similar arrestin scaffold with
398 arrestin which contains a semi-symmetric fold of two β strand sandwich structures in the N domain
399 and C domains linked by the central loops with each sandwich formed by 3 or 4 β sheets,
400 respectively.

401 For arrestin, the conserved structures mainly include the N-terminal and C-terminal arm,
402 central crest comprised of a finger loop (Hirsch et al., 1999), a middle loop (Kim et al., 2012;
403 Shukla et al., 2013); see box ii of Fig. 4) and C loop (Kang et al., 2015) see box I of Fig. 4), Figure
404 4A), the gate loop, polar core, and the hinge domain (Peterson and Luttrell, 2017). The N-terminal
405 and C-terminal arms stabilize the arrestin conformation. Model atvps26a-2 shares similar N-
406 terminal and C-terminal scaffolds with arrestin however it lacks a short α-helix inside the arrestin
407 N-terminal domain (Figure 4B) which has been implicated in receptor binding (Vishnivetskiy et
408 al., 2011). In addition, arrestin has a longer C-terminal tail, which extend all the way to bind the
409 N terminal domain, important for linkage to enable CME. The C terminus of atvps26a-2 has no
410 extension however some arrestins also have a short C-tail (Gurevich and Gurevich, 2006).

411 The overall central crest of atvps26a-2 is similar with that of arrestin which includes the
412 finger loop, middle loop and the C loop (Figure 4C). While arrestin has a longer finger loop
413 important for receptor binding. The rearrangement of the finger loop is a major change associated
414 with arrestin activity, likely serving as a critical part of the activation sensor (Chen et al., 2018).

415 The polar core is the key component of the phosphate sensor. In arrestin, the polar core is
416 comprised of five charged side chains including two Arg and three Asp that are essential to its
417 activation (Vishnivetskiy et al., 1999). The residues in the polar core of bovine arrestin-3 are:
418 Asp_{27}, Arg_{170}, Asp_{291}, Asp_{298} and Arg_{393} (Figure 4D and E). The human vps26A also contains a
419 polar core between the N terminal and C terminal domains which includes the N domain residues
420 Glu_{119} and Tyr_{121}, and C domain residues Lys_{213}, Glu_{215}, Thr_{258}, Tyr_{272}, and Arg_{296} (Shi et al.,
421 2006). The residues of the polar core of VPS26 are conserved suggesting that they play a critical
422 role in protein function. We thus labeled the polar core of atvps26a according to the human vps26a
423 template. The residues of atvps26a are the N-domain residues Glu_{118} and Tyr_{120}, and C domain
424 residues Arg_{213}, Glu_{215}, Thr_{258}, Tyr_{272}, and Arg_{296} (Figure 4 F and G). Although different amino
425 acid composition, both cores consist of positive charged residues and allow the formation of
426 hydrogen bonds under physiological conditions. However, the orientation and shape of the polar
427 core of VPS26 is distinct from arrestin. The arrestin polar core is embedded between β sheets in
428 the N terminal domain whereas the VPS26 core is open and elongated, spanning the length of
429 space between the N domain and C domain.

430 The most divergent arrestin structure from 3P2D is a 3Å-resolved truncated arrestin from
431 squid (PDB 1CF1, (Bandyopadhyay et al., 2018). Unlike for bovine arrestin, the C-tail interaction
432 with the gate loop of the polar core is weak and flexible. This functional divergence between

433 squid and human arrestin, both recruited to receptors, tempers the impact of the lack of a long C-
434 tail in the atvps26a-2 model.

435 Taken together, these similarities between AtVPS26 and arrestin prompted the hypothesis
436 that AtVPS26 is a candidate adaptor for CME of AtRGS1. Therefore, we isolated null alleles of
437 the three VPS26 genes in Arabidopsis: VPS26A, VPS26B, and VPS26-LIKE (aka VPS26C) (Jha
438 et al., 2018; Zelazny et al., 2013) and phenotyped the hypocoty length at 5 days, the relevant stage
439 for our cytological analyses. As shown in Figure S4F, there were no qualitative differences
440 between VPS26 null mutants and Col-0 precluding any developmental basis for alterations in
441 AtRGS1 activation in these mutants. In addition, the AtRGS1-YFP reporter was combined with
442 the mutant backgrounds through generating stable transformants. As shown in Figure 4H, loss of
443 either VPS26A or VPS26B dramatically reduced the flg22-induced internalization of AtRGS1 to
444 levels that are not statistically different from the baseline level ($p=0.34$) whereas loss of VPS26-
445 like had no statistical effect on AtRGS1 internalization by flg22 ($p=0.65$). Loss of any of the three
446 VPS26 proteins had no statistical effect on glucose-induced internalization of AtRGS1 ($p<0.001$)
447 suggesting that VPS26A/B are involved in flg22- but not glucose-induced AtRGS1 endocytosis.
448 To confirm that VPS26 is not involved in glucose-induced AtRGS1 internalization, we quantitated
449 the CME and SDE portions of this trafficking pathway in the *vps26* mutants. As shown in Figure
450 4I, in each of the *vps26* mutant backgrounds, both the TyrA23A and MβCD-inhibitable segments
451 of the glucose-induced internalization of AtRGS1 remained intact. This suggests that the TyrA23-
452 dileneated (CME) pathway used by AtRGS1 when activated by flg22 differs from the TyrA23A-
453 dileneated pathway activated by D-glucose.

454 The genetic data suggest that VPS26A and B form dimers. To test if VPS26 A and B
455 subunits heterodimerize *in vivo*, BiFC analysis was conducted and showed that heterodimers can

456 form from ectopically-expressed monomers and suggested that the orientation is head-to-tail
457 (Figure 5A). Self-association of arrestin family members also occurs and may be part of a
458 regulatory mechanism for arrestin activation (Chen et al., 2014). For relative quantitation of *in*
459 *vivo* interaction, split luciferase was performed and found that the strongest interaction was
460 between VPS26A and VPS26B (Figure 5B). VPS26B dimers form under these conditions but not
461 VPS26A dimers or any oligomer with VPS26Like subunits. We have yet to find conditions which
462 allow stable expression of VPS26 subunits tagged with a full-length auto-fluorescent protein in
463 Arabidopsis suggesting that the additional mass of the tag prevents dimer formation and that
464 monomers are unstable.

465 To test if the full-length AtRGS1 protein interacts with the VPS26 subunits *in vivo*, BiFC,
466 split luciferase, and Y2H analyses were performed. Fluorescent complementation of YFP by
467 AtRGS1-nYFP with cYFP-VPS26A and with VPS26B-cYFP was observed (Figure 5C). The split
468 luciferase assay confirmed that this interaction is as strong as the interaction between AtGPA1 and
469 its AGB1/AGG1 partner (Figure 5D). Finally, Y2H showed that the interaction between AtRGS1
470 and VPS26 is direct. The entire C-terminal half of AtRGS1 (thus lacking the 7 TM domain)
471 interacts with VPS26B. Surprisingly, removal of the post RGS-box C-terminal tail which includes
472 the $Ser_{428,435,436}$ phosphorylation cluster did not ablate this interaction however, additional loss of
473 two other phosphorylated Ser located between helices VII and VIII of the RGS box completely
474 abolished the interaction.

475

476 **Biased Signaling Outputs**

477 While both D-glucose and flg22 result in different RGS1-YFP trafficking, we asked what other
478 signaling outputs distinguish these ligands. Two rapid events of the flg22 response is the induction

479 of MITOGEN ACTIVATED PROTEIN KINASE 6 (MPK6) activity and Ca^{2+} signaling (Ranf et
480 al., 2011). To test the impact of flg22 and D-glucose on MPK6 activity in etiolated hypocotyls, we
481 developed a FRET-based sensor that measures kinase activity specifically for MPK6, called *S*ensor
482 *O*f *M*APK *A*ctivity (SOMA) (Zaman et al., 2019). We used SOMA lines tagged with either the
483 human immunodeficiency virus 1 (HIV-1) nuclear export signal (SOMA-NES) or the SV40
484 nuclear localization signal (SOMA-NLS) (Kalderon et al., 1984; Wen et al., 1995) to measure
485 MPK6 activity in the cytosol or nucleus, respectively. To validate these reporters in hypocotyl
486 epidermal cells, we quantitated FRET efficiency in the SOMA lines in response to 150 mM NaCl
487 as a positive control (Droillard et al., 2004). FRET efficiency increased rapidly in SOMA-NES
488 and SOMA-NLS in response to NaCl with no response observed when treated with water (Fig S6
489 A-D). Additionally, flg22 treatment did not cause substantial FRET efficiency changes in negative
490 control reporter lines: $SOMA^{T679A}$-NES or $SOMA^{T679A}$-NLS, which contain mutations in the
491 known phosphorylation site of SOMA that are necessary for FRET changes (Fig S6 E, F). As
492 shown in Figures 6E and F, rapid FRET gains were observed in both SOMA-NES and SOMA-
493 NLS within 2-4 minutes after treatment with flg22. When treated with 6% D-glucose, no change
494 in FRET efficiency was observed, suggesting that D-glucose does not induce activity of MPK6
495 (Fig 6G and H).

496 To determine if CME-mediated endocytosis regulates flg22-induced MPK6 activity, we
497 pretreated SOMA-NES lines with TyrA23. TyrA23 successfully blocked the increases in FRET
498 efficiencies that were observed in the absence of the inhibitor (Fig 6E, replicates in Fig S6 G-N).
499 The negative control TyrA51 showed no significant effect on FRET efficiency after treatment with
500 flg22 (Fig S6 P-V), indicating that the inhibitory effect of TyrA23 is specific to its role in blocking
501 CME-mediated endocytosis and suggesting that AtRGS1 endocytosis, per se, is required.

502 However, we do not exclude the possibility that within the context of flg22-induced MAPK
503 signaling that some other CME-mediated step is rate-limiting.

504 Because D-glucose utilizes both CME and sterol-dependent pathways to induce AtRGS1
505 internalization, we tested if the depletion of CME pools of AtRGS1 by D-glucose would alter
506 flg22-induced MPK6 activation. After pretreating SOMA-NES lines with D-glucose for 30
507 minutes prior to imaging, we found that D-glucose did not have an effect on flg22-increased FRET
508 efficiency (Fig 6G inset) suggesting that the glucose pool of AtRGS1 is sequestered from the flg22-
509 induced CME of AtRGS1.

510 We tested the role of D-glucose and flg22 in triggering an increased Ca^{2+} transient response
511 using the intensity-based Ca^{2+} sensor R-GECO1, a red-shifted intensity-based Ca^{2+} reporter
512 (Keinath et al., 2015). We used stable transgenic Arabidopsis lines in wild type and *rgs1-2*
513 backgrounds expressing cytosolic- and nuclear-localized R-GECO1. For our assay, D-glucose and
514 flg22-induced Ca^{2+} signals in wild type and *rgs1-2* plants were measured over a time course in
515 etiolated hypocotyls and normalized against the untreated samples (Fig 6I and 6J). Ca^{2+} levels
516 represented by fractional fluorescence changes ($\Delta F/F$; the difference between the fluorescence
517 intensity before and after flg22 application divided by initial fluorescence intensity) increased in
518 wild type ($p < 0.01$) while $\Delta F/F$ was greatly diminished ($\Delta F/F = \sim 0.01$) in the *rgs1*-2 mutant in
519 response to flg22. D-glucose treatments did not significantly alter the $\Delta F/F$ in Col-0 wild type or
520 *rgs1*-2 mutant ($p=0.62$), suggesting that D-glucose does not utilize AtRGS1 in a Ca^{2+} branch of the
521 pathway. Despite both D-glucose and flg22 inducing AtRGS1-internalization, these results show
522 that within this context, only flg22 is capable of inducing MPK6 activity and Ca^{2+} changes.

523 Here, we showed that D-glucose signaling mediated by AtRGS1 does not involve MAPK
524 or Ca^{2+} branches, however, D-glucose has been shown to elicit a change in expression of a small

525 set of genes (Grigston et al., 2008; Urano et al., 2012). *TRICHOMELESS LIKE 26* (*TBL26*) is
526 induced by glucose in an AtRGS1/G protein complex-dependent manner (Grigston et al., 2008)
527 and has since been used as a reporter for activation (Fu et al., 2014; Urano et al., 2016; Urano et
528 al., 2012). Paradoxically, the loss of AtRGS1 inhibits *TBL26* expression indicating that genetically,
529 AtRGS1 is a positive modulator of signaling, contradictory to our understanding that RGS proteins
530 negatively modulate G protein activation. One solution to this paradox is that endocytosis of
531 AtRGS1 is required for signal propagation. To test this, we quantitated glucose-induced *TBL26*
532 expression in the presence of TyrA23 and found that expression is dramatically reduced (Fig 6L).
533 This is consistent with the notion that AtRGS1 signaling has an endosomal origin, analogous to
534 some GPCRs (Eichel and von Zastrow, 2018).

535 **DISCUSSION**

536 The key finding in this study is system bias wherein a single receptor-like RGS protein modulates
537 different quantifiable signaling outputs from two distinct signal inputs (Figure 7A). All of the
538 measured signal outputs correspond to a specific ligand input. For example, flg22 induces Ca^{2+}
539 release (Figure 6I-K) and MAPK signaling (Figure 6E-H, K) whereas D-glucose or its metabolite
540 has a measured effect on gene expression (Figure 6L). For flg22, all members of the G protein
541 heterotrimer, along with XLG2 and VPS26A/B are necessary for CME of AtRGS1. Additionally,
542 specific phosphorylation of di-serines at the AtRGS1 C-terminus is required. What is interesting
543 is that glucose signaling that transduces through the same CME of AtRGS1 also requires
544 phosphorylation of the same di-serine residues, but not VPS26 for high dose and low duration
545 sugar exposure (Figure 7B). This phenomenon of signaling through AtRGS1 mediated by the same
546 mechanism of phosphorylation-dependent endocytosis with different G proteins and adapters
547 raises the important question of how are extracellular ligands discriminated for downstream

548 signaling events? Although AtRGS1 endocytosis is necessary for G protein activation it would
549 seem that AtRGS1 is not the discriminator; rather an RLK protein that directly phosphorylates
550 AtRGS1, AtGPA1 and possibly VPS26, to provide the requisite information for ligand-specific
551 downstream signal transduction in the cell.

552 The two mechanisms of AtRGS1 endocytosis induced by D-glucose or its metabolites
553 implies that this signal-dependent pool of AtRGS1 is bipartite, prompting the question of an
554 equilibrium or steady state between the populations. The evidence so far suggests that it is not. If
555 these AtRGS1 pools were dynamically exchanging within the membrane, we would expect to
556 induce internalization of nearly all membrane bound AtRGS1 by inhibiting one mechanism of
557 endocytosis thereby causing a shift entirely to the other. For example, inhibiting CME with
558 TyrA23 would force AtRGS1 endocytosis entirely to the SDE mode, however this was not
559 observed. Inhibiting one mechanism of endocytosis only partly reduced AtRGS1 internalization
560 by half, indicating the AtRGS1 populations may be physically isolated and static in the cell
561 membrane (Figure 7C). Some AtRGS1 proteins may be grouped into so-called microdomains or
562 clusters surrounded by receptor/co-receptor RLK proteins while other AtRGS1 may be distributed
563 throughout the membrane without common neighbor RLKs (Figure 7C).

564 Similarly, the question exists whether an equilibrium between the flg22-mediated and D-
565 glucose-mediated CME pools exists and the conclusion is again that equilibria are not likely,
566 consistent with a genuine bias in signaling. To clarify, what we define as the "CME pools" here,
567 they are the portion of either the flg22- or D-glucose-activated AtRGS1 population that is inhibited
568 by TyrA23, by loss of the tyrosine binding motif, and by loss of the AP2μ subunit of the clathrin
569 complex (Figure 2). While the two pools share these properties, they do not share the requirement
570 of the candidate adapter, VPS26 monomer or dimer (Figure 4). Moreover, when the AtRGS1 pool

571 at the plasma membrane is depleted with D-glucose, there is no effect on the amplitude of flg22
572 activation (Figure 6).

573 The two mechanisms in the composite glucose-induced AtRGS1 endocytosis may be a
574 result of two distinct mechanisms of sugar perception: one through direct interaction of AtRGS1
575 with a sugar or sugar metabolite and the other through sugar binding to a RLK in the membrane
576 similar to flg22::FLS2 binding (Figure 7D). To compare and contrast these two ligand-biased
577 trajectories, the ordered steps of signal transduction from ligand perception (**step 1**) to
578 internalization of AtRGS1 (**step 5**) are enumerated in Figure 7D to illustrate mechanistically what
579 the present work revealed about each origin of endocytosis including phosphorylation (flg22- **step**
580 **2**/glucose- **step 2**), binding of our candidate adaptor VPS26 (flg22- **step 3**), formation of clathrin
581 coated vesicles (flg22- **step 4**/glucose- **step 3**), and finally endocytosis of AtRGS1 either via
582 clathrin coated vesicle (flg22- **step 5/** glucose **step 4**) or sterol dependent rafts (glucose). If glucose
583 or a metabolite is perceived by two distinct sensing mechanisms, each mechanism may operate
584 exclusively through one origin of endocytosis with a unique core of G protein and internalization
585 signaling components. Interestingly, within the glucose model, a system bias may exist favoring
586 one origin of endocytosis that results from architectural differences in the membrane surrounding
587 AtRGS1. A high density of glucose-binding RLKs may favor glucose-induced CME of AtRGS1
588 over the SDE origin.

589 The division of G protein involvement in glucose-induced CME and SDE challenges
590 previously published reports on the necessity for subunits of the G protein heterotrimer in the full
591 range of glucose signaling through AtRGS1; specifically shown was the complete abrogation of
592 AtRGS1 endocytosis in the Gβ null mutant and partial reduction of glucose-induced endocytosis
593 with the loss of Gα (Urano et al., 2012). Our results confirm that Gβ is required for AtRGS1

594 endocytosis, but only in a low dose scenario, 2% (~110 nM). We show no requirement for Gβ or
595 Gα at the higher 6% (~330nm) glucose concentration. It may be that higher sugar concentrations,
596 those typically found at or around vascular unloading areas, illicit a quicker signaling response
597 than low dose sugar likely found in or near epidermal cells where we quantified AtRGS1
598 internalization. The significance of sugar signaling with regard to cell growth, division, and
599 maintenance may necessitate multiple dose-dependent mechanisms of signal transduction encoded
600 in different origins of endocytosis and the individual G protein associated components.

601 Both flg22- and D-glucose outputs require AtRGS1 (Chen et al., 2003; Grigston et al.,
602 2008; Liang et al., 2018; Tunc-Ozdemir and Jones, 2017) and an intact heterotrimeric G protein
603 complex (Figure 3) but as discussed for D-glucose responsiveness, the outputs depends on both the
604 concentration and duration of D-glucose. We previously designated this non-threshold-based
605 activation phenomenon as Dose-Duration Reciprocity (**DDR**) where a low dose of D-glucose for
606 a long period reaches the same output amplitude as a high dose presented as a pulse (Fu et al.,
607 2014). The proposed mechanism is recruitment of WNK8 and WNK1 to the membrane by the
608 Gβγ dimer AGB1/AGG as a function of DDR to phosphorylate AtRGS1 for endocytosis.
609 However, our higher resolution analyses here challenge some aspects of that mechanism and
610 provide deeper mechanistic insight. AGB1 is essential for low D-glucose DDR but is not required
611 for high-glucose DDR. WNK8 kinase is required as previously shown but WNK1 is shown to not
612 be required at longer low-glucose treatments (6 hours) in contrast to previously published data (Fu,
613 et al 2014). This discrepancy is most likely due to differences in expression level between studies
614 (transient for Fu, et al 2014 and stable here) because glucose responsiveness is sensitive to the
615 pool size of AtRGS1 (Liao et al., 2017).

616 Besides the 2 visual and 2 non-visual (aka β-) arrestins, the arrestin super family in humans
617 also has 6 α-arrestin members. These α–arrestins have diverse functions including trafficking of
618 non-GPCRs (Patwari and Lee, 2012) and may be closest to the ancestral arrestin from which the
619 visual/non-visual arrestins evolved because they are found in stromenopiles basal to the opistokont
620 lineage containing metazoans and fungi (Alvarez, 2008). Therefore, we asked whether Plantae
621 contains α–arrestin homologs and are thus the true adaptors for trafficking plant 7TM proteins.
622 While we found clear α–arrestin orthologs in the 4-cell alga *Tetrtabaena* (PNH03120) and in the
623 green alga *Chara* (GBG71752), both basal to land plants, using *Mus* ARRDC3/TLIMP (BAC65781)
624 as the search query, no hits were found in Arabidopsis (eudicot), *Amborella* (base of angiosperms),
625 rice (monocot), and *Physcomitrella* (basal to higher land plants). This suggests that α–arrestins
626 were lost in the plantae kingdom and this loss possibly allowed expansion of the related VPS26
627 family to evolve other function(s) (Alvarez, 2008).

628 Given the fact that many GPCR-containing organisms divergent to humans lack arrestin
629 proteins, another important finding from this study is the suggestion that the retromer subunits
630 AtVPS26A and B moonlight as arrestin-like adaptors for phosphorylation-induced, clathrin-
631 dependent AtRGS1 endocytosis in Arabidopsis. Could this function be ubiquitous? Even in
632 humans, some GPCR endocytosis occurs independently of β-arrestins yet still requires C-terminal
633 phosphorylation, a tyrosine motif, AP2, and clathrin (e.g. (Paing et al., 2002; Smith et al., 2016))
634 raising the possibility that VPS26 orthologs in humans may serve the exact adaptor function for a
635 subset of GPCRs.

636 This study focuses on biased signaling launched from different architectures of two
637 AtRGS1-centered pathways. We show that phosphorylation by different sets of kinases encodes
638 this bias. However, we have not address how the architecture is established or maintained but we

639 speculate that this too is based on a phosphorylation bar code on the AtRGS1/G protein complex.
640 Therefore, establishing the dynamics of both the pre- and post-signaling phosphorylation bar codes
641 is important for our understanding of biased system signaling.

642 Why both cytoplasmic and extracellular glucose pools are monitored by the plant cell
643 remains unclear. We speculate that the extracellular pool of glucose is far more dynamic than the
644 cytoplasmic pool due to its rapid metabolic flux in the cytoplasm compared to the apoplast.
645 Therefore, an extracellular glucose detection system may be more appropriate for monitoring
646 sugars produced by photosynthesis for real time information. This is consistent with the recent
647 finding that AtRGS1 is important for detecting fluctuations in CO_2-fixed sugar in the minute time
648 range over the diel cycle (Chen et al., 2003; Tunc-Ozdemir et al., 2018).

649 It is conceivable that this biased system sits at the crux of the "defense vs. growth trade-
650 off" dilemma that plants face. Specifically, pathogen attack compels the plant to shift its utilization
651 of fixed sugars from building cell walls to synthesizing defense molecules (Huot et al., 2014). The
652 AtRGS1/G protein complex may be the fulcrum for this balance because AtRGS1 is involved in
653 detecting fixed sugars (Mudgil et al., 2016; Tunc-Ozdemir et al., 2018), establishing cell wall
654 composition (Delgado-Cerezo et al., 2012; Escudero et al., 2017; Klopffleisch et al., 2011) and
655 serving as a sentinel in innate immunity (Zhong et al., 2018).

656 In conclusion, our data provide evidence for system biased signaling through AtRGS1 and
657 introduces a previously unknown arrestin-like adaptor. We introduce the importance of system
658 architecture as it relates to system bias in G protein complex signaling.

659

660

661 **MATERIALS AND METHODS**

662 *Chemicals.*

663 Methyl-β-cyclodextrin was purchased from Frontier Scientific, tyrphostin A51 and turanose were
664 purchased from Sigma-Aldrich, and tyrphostin A23 was purchased from Santa Cruz
665 Biotechnology. All chemicals were indicated by the vendors to be >98% pure.

666

667 *Plant Growth Conditions*

668 Arabidopsis seeds were surface sterilized with 80% EtOH for 10 seconds while vortexing followed
669 by a 10-second vortex with 30% bleach. Seeds were subsequently washed 3X with ddH_20 and
670 suspended in 12 well cell culture plates with ¼ MS with no sugar at pH 5.7 with 10-12 seeds per
671 well. Plates were wrapped in aluminum foil and cold-treated at 4˚C for 2 days followed by a 2-
672 hour light treatment to induce germination. After light treatment, plates were again wrapped in
673 aluminum foil and placed on a horizontal shaker at ambient temperature for 5 days before imaging.

674

675 *AtRGS1 Internalization Assay, Proxy for G protein activation*

676 AtRGS1-YFP internalization was induced with D-glucose and flg22 as described (Fu et al., 2014;
677 Tunc-Ozdemir et al., 2016; Urano et al., 2012). Briefly, wild type (Col-0) Arabidopsis seeds
678 expressing 35S:AtRGS1-YFP were sterilized and then sown on 1-mL liquid 1/4 X Murashige and
679 Skoog (MS) medium without sugar in 12-well plates and stratified at 5ºC for 2 days, followed by
680 2 hours light, then grown in darkness at RT for 3-5 days. For optimal results, the plates were kept
681 in darkness but moved to the microscope room on the third day to acclimate. 6% D-glucose or 1µm
682 flg22 were applied to seedlings for 30 and 10 minutes respectively before imaging. Image
683 acquisition was done on either a Zeiss LSM710 (Zeiss Microscopy, Oberkochen, Germany) with

684 a C-Apochromat 40X 1.2NA water immersion objective (for figures 2A-2I and figure 3A-3D) or
685 a Zeiss LSM880 with a C-Apochromat 40x/1.2NA water immersion objective (for figure 2K-2P,
686 3E-3K, and S3). YFP excitation was at 514nm and emission collection 525-565nm. Emission
687 collection on the LSM880 was done with a GaAsP detector. For RGS internalization assays a z-
688 stack series was acquired at 0.5µm intervals between images. Image processing and RGS
689 internalization measurements were done with the Fiji distribution of ImageJ (Schindelin et al.,
690 2012) as described by Urano *et al (Urano et al., 2012)* with the following modification:
691 Internalized YFP fluorescence was measured and subtracted from total YFP fluorescence of
692 individual cells as opposed to total fluorescence of the hypocotyl image as stated in Urano *et al*.
693 Images were acquired on the hypocotyl epidermis 2-4 mm below the cotyledons of seedlings
694 treated with water, glucose, and flg22 in addition to the pharmacological inhibitors. Seedling
695 exposure to light was minimized as much as is practical while imaging to avoid light induced
696 internalization of AtRGS1. Statistical analysis was performed using analysis of variance with
697 n=number of cells measured. Differences in basal and treatment induced levels of RGS1-YFP
698 internalization are a result of switching image acquisition from the LSM710 to the LSM880 to
699 improve image resolution and accuracy of internalization measurements.
700
701 *Pharmacological Inhibition of RGS Internalization*
702 AtRGS1 internalization was inhibited with TyrA23 and MβCD under the following conditions.
703 TyrA23 was applied to 3-day old seedlings for a pre-incubation period of 60 minutes at specified
704 concentrations. Following the pre-incubation period, a combination of TyrA23 and 6% D-Glucose
705 were applied to the seedlings for 30 minutes immediately followed by image acquisition. In the
706 case of flg22, TyrA23 and 1µm flg22 were applied to the seedling for 10 minutes following the

707 pre-incubation period. For MβCD, the pre-incubation period was 45 minutes at specified
708 concentrations. When both inhibitors were simultaneously applied, pre-incubation was 60 minutes
709

710 *TIRF imaging and area/speed measurements of AtRGS1-GFP*

711 Arabidopsis Col-0 seeds containing 35S-RGS1-GFP were grown as mentioned in the plant growth
712 section. 5-day-old seedlings were transferred to a solution of either 6% D-glucose or 1µm flg22
713 and imaged at 5, 10, and 15 minutes while immersed in the ligand solution. Imaging was performed
714 on a Nikon Ti Eclipse with SR Apo TIRF 100x lens (NA 1.5, WD 120µm). GFP excitation
715 occurred at 488nm and emission collection at 515-555nm with an Andor iXon3 EMCCD camera.
716 60 second time-lapse imaging was initiated at the beginning of each time point with 200ms
717 acquisition speed. Time-lapse sequences were normalized for fluorescence over time using
718 IMARIS (v9.2.2, Bitplane AG, Zurich, Switzerland). The IMARIS Surface feature was used to
719 track and calculate the area and speed of individually identifiable AtRGS1 proteins/clusters
720 (labeled as tracks in IMARIS) over time. The average speed and area of each unique track for a 30
721 second interval between 5:15-5:45 or 15:15-15:45 was calculated using a script in Matlab
722 (Supplemental code).
723

724 *Synthesis of [^{14}C] isomaltulose*

725 Sucrose isomerase (SI) from *Pantoea dispersa* UQ68J (GenBank AY223549) was cloned into
726 expression vector pET24b (Novagen) first by PCR of genomic DNA using the following PCR
727 forward primer 5'-GGA TCC AAC AAT GGC AAC GAA TAT ACA AAA GTC C-3' which
728 included a *BamHI* restriction site and a start codon; reverse primer 5'-ATA GGT ACC TCA GTT
729 CAG CTT ATA GAT CCC-3' which included a *KpnI* restriction site and a stop codon.

730 Expression was performed using *E. coli* BL21(DE3) (Novagen), 37°C, 225 rpm. When
731 the optical density at 600nm reached 1.00, isopropyl-D-thiogalactopyranoside was added to a final
732 concentration of 0.5 mM for induction. The incubation of the culture was continued for another 3
733 h at 28°C. Cells were harvested by centrifugation (3,000 ×g, 4°C, 10 min), resuspended in 50 mM
734 Tris-HCl (pH 8.0)-2 mM EDTA, and then re-centrifuged. The cell pellet was immediately frozen
735 in liquid nitrogen and stored at -75°C. Cells were suspended in extraction buffer (20 mM Tris-HCl
736 (pH 7.4), 200 mM NaCl, 1 mM EDTA, 1 mM azide, 10 mM β-mercaptoethanol) and then lysed
737 by sonication (nine 15-s pulses at 50 W with a Branson Sonifier 450 microprobe), centrifuged
738 (10,000 ×g, 4°C, 10 min), and filtered through a 0.45-µm-pore-size membrane (Gelman Acrodisc).
739 The pET24b vector introduced a carboxy-terminal six-His tag into expressed proteins, which were
740 purified by adsorption to nitrilotriacetic acid (NTA) agarose (QIAGEN) and elution with 25 mM
741 NaH2PO4-150 mM NaCl-125 mM imidazole buffer (pH 8.0) by following the manufacturer's
742 instructions. The purity of SI proteins was verified by SDS-PAGE as a single band on Coomassie
743 Blue R-250 staining.
744 [^{14}C] isomaltulose was prepared using 1.48MBq [U-^{14}C]Sucrose (Amersham, UK) in 200
745 µl water with 3% ethanol (equals to 0.3379 mM) was reacted with 30 µl purified UQ68J SI for at
746 30 °C 60 min. The converted [^{14}C] isomatulose concentration by UQ68J SI was estimated by three-
747 replicate parallel conversions of unlabelled sucrose (S7903,Sigma) in the same concentration of
748 0.3379 mM with 3% Ethanol by the same enzyme. BioLC DX600 (Dionex, USA) determinations
749 showed 84.0±0.106% (Mean±SE) was converted into isomaltulose, 3.5±0.197% into trehalulose;
750 into the by-products of glucose and fructose were 4.6±0.072% and 7.8±0.237% respectively and
751 there was no sucrose left after the reaction was stopped (Figure 1A).
752

753 *Sugar uptake assay*

754 One-week-old seedlings, grown on a filter disc overlaying 1/2X Murashige and Skoog Basal Salts,
755 0.7% phytogel 23ºC, pH 5.8, 8h/d of 100 mole/m2/s1, were lifted off the plate and overlaid 6 mL
756 of water containing approx. 25,000 cpm of [^{14}C] sugars as indicated. The specific activity of the
757 sugars was 12GBq/mmol. At the indicated times, triplicate sets of 10 seedling were gently rinsed
758 and placed in a 1.7-mL microfuge tube with 1 mL of scintillation fluid (Perkin Elmer Inc) and
759 radioactivity was quantitated by liquid scintillation counting. CPM from time zero (typically 80-
760 150 cpm) was subtracted from the average of the 3 samples. The CPM for [^{14}C] isomaltulose
761 uptake into seedlings at each time was corrected for its 84% purity. The experiment as shown was
762 repeated once with the same result. [^{14}C] glucose uptake was repeated 4 times.

763

764 *Live cell imaging of MAPK reporter (SOMA) lines*

765 Detached etiolated hypocotyls were prepared for imaging on the confocal microscope using the
766 HybriWell™ method as previously described (Vang et al., 2018; Zaman et al., 2019). A hypocotyl
767 from a dark grown 5-day-old seedling was placed on top of the droplet, and a HybriWell™ (Grace
768 BioLabs, http://gracebio.com/, cat. no. 611102) was gently placed on the coverslide with the
769 hypocotyl in the center to form a 150-µm deep imaging chamber with a volume of 30 µl. Ultrapure
770 water (300 µl) was injected through one of the HybriWell™ ports using a pipettor to fill the 30-µl
771 chamber with water and to expel any air bubbles. A 200-µl droplet of ultrapure water was then
772 placed on one of the ports to prevent the chamber from drying out. The HybriWells containing the
773 mounted hypocotyls were then placed in covered Petri dishes and equilibrated by incubating at
774 20–23°C under constant light for 6–8 hours prior to imaging.

775 Confocal microscopy was performed using a Zeiss LSM 710 with a C-Apochromat
776 40x/1.20 water immersion objective lens. Samples were excited at 458nm with 3% power, and
777 emission was measured between 463 and 517nm for Turquoise GL and between 534 and 570nm
778 for YPet. Z-stacks were collected every 2 min with an optical slice thickness of 1.2 µm. Chemical
779 treatments were added to the samples during imaging by pipetting 200 µl of solution containing
780 the treatment onto one port of the HybriWell. For experiments involving tyrphostin A23 and
781 tyrphostin A51, hypocotyls were pretreated with 50 µM of these compounds for 30 min prior to
782 imaging.

783 Post-processing of the raw image data was performed using Fiji (Schindelin et al., 2012).
784 The 'Z-projection' function was performed on an image stack using the 'Max Intensity' setting.
785 The resulting projection was then separated into two images, one for the Turquoise GL emission
786 channel and one for the YPet emission channel. The 'Subtract Background' function was
787 performed on both images, with the 'rolling-ball radius' set as the default 50 pixels. A mask was
788 then created from the YPet channel using the 'Convert to Mask' function. The background
789 subtracted YPet and Turquoise GL images were then converted into 32-bit images. These 32-bit
790 images were then multiplied by the Mask file. The resulting YPet image was divided by the
791 resulting Turquoise GL image using the 'Image Calculator' function to create a ratio image
792 representing the ratio of YPet to Turquoise emission. Finally, the 'Threshold' function was
793 performed using the default values, with the 'NaN background' option enabled. The 'Fire' lookup
794 table was then applied to the final ratio image. To measure the ratio of YPet to Turquoise GL
795 emission, a region of interest (ROI) was selected within the ratio image using Fiji and the average
796 ratio value within that ROI was then measured.

797 *Live cell Ca^{++} imaging with R-GECO1*

798 5-day-old etiolated hypocotyls expressing R-GECO1 calcium reporter were grown in aqueous
799 media containing ¼ MS. Hypocotyls were excised and mounted in HybriWells 6-8 hours prior to
800 imaging with a Zeiss LSM710 confocal laser scanning microscope equipped with a C-Apochromat
801 40×/1.20 water immersion objective. R-GECO1 was excited using 561nm laser with 7.0 % laser
802 power, and emission was measured between 620 and 650 nm. Z-stacks were collected 2 min after
803 chemical treatment with an optical slice thickness of 1.5µm. Chemical treatments were added to
804 the samples during imaging by pipetting 200 µl of solution containing the treatment onto one port
805 of the HybriWell. The digital images were analyzed with Fiji (Schindelin et al., 2012).

806 *Modeling AtVPS26*

807 Five models (atvps26a1-5) were created by the MODELLER using the automodel script based on
808 the human VPS26A template 2FAU. For evaluation and selection of the "best" model, we
809 calculated the objective function (molpdf), Discrete Optimized Protein Energy (**DOPE**) score,
810 GA341 assessment score and root mean square deviation (**RMSD**) between the model and the
811 template. The best model has the lowest value of the molpdf and overall DOPE assessment scores.
812 In addition, DOPE scores were calculated per-residue and the template and the five atvps26a
813 models were compared using GNUPLOT (Figure S4C) and found to be dissimilar in only three
814 positions (residue around 60, 240, and 260). The atvps26a2 model was selected based on the
815 lowest, RMSD value (Figure S4D) and plotted DOPE per-residue score curve (Fig. S4E). With an
816 RMSD of 0.17 Å, atvps26a-2 differs from the template by less than the length of a C-C bond.

817 *Split firefly luciferase assays*

818 pCAMBIA/des/cLuc and pCAMBIA/des/nLuc (Lin et al., 2015) were used to generate the
819 following plasmids: AtVPS26A-nLUC, AtVPS26B-nLUC, cLUC-AtVPS26A, cLUC-AtVPS26B,
820 cLUC-AtVPS26like, cLUC-AtGPA1, AtAGB1-nLUC and AtRGS1-nLUC. pART27H-mCherry-

821 AtAGG1 plasmid was obtained from Dr. Jose R Botella (University of Queensland, Brisbane,
822 QLD, 4072, Australia). All plasmids were transformed into *A. tumefaciens* strain *GV3101*. nLUC
823 and cLUC fusion partners were co-expressed in *N. benthamiana* leavesby agroinfiltration
824 following protocols in (Zhou et al., 2018). 48 hours after infiltration, 6mm Leaf discs were
825 collected to 96-well plate and 40µl 0.4mM D-luciferin was added to each well. Luminescence was
826 measured by spectraMax L microplate reader (Molecular Devices).

827 *Yeast two-hybrid assays*

828 Constructs used in yeast two-hybrid assays were pAS–RGS-J5 (amino acids 284–459), RGS-ΔCt
829 (amino acids 284–416), RGS-ΔCtS405,406A, pACTGW–AtVPS26B and AtVPS26like. Y2H
830 tested pairs were co-transformed into *AH109* yeast cells and plated on SD-LW media (Wagemans
831 and Lavigne, 2015). Colonies were then inoculated into SD-LW liquid media and grew overnight
832 at 30 °C. Then 1/10 diluted yeast cells were spotted on SD-LW, SD-LWH, and SD-LWH 10mM
833 3-AT (3-amino-1,2,4-triazole) plates. The plates were incubated at 30°C for 4 days and were
834 imaged by gel documentation system (Axygen) under white light.

835

836 **SUPPLEMENTAL INFORMATION**

837 Supplemental Information includes 6 figures and 1 text file.

838

839 **ACKNOWLEDGEMENTS**

840 We would like to thank Dr. N Phan for creating the AtRGS1^{Y112A} plasmid and transgenic lines and
841 for experiments testing the involvement of adaptors in AtRGS1 endocytosis and data in Figure 1A
842 and B. We thank Dr. V Gurevich, Dr. M Garcia-Marcos and Dr. CE Alvarez for helpful comments
843 and Dr. K Ghusinga for assistance with writing MatLab code. We thank Dr. J Huang for help in

844 the turanose experiment. This work was supported by grants from the NIGMS (GM065989) and
845 NSF (MCB-1713880) to A.M.J. The Division of Chemical Sciences, Geosciences, and Bio-
846 sciences, Office of Basic Energy Sciences of the US Department of Energy through the grant DE-
847 FG02-05er15671 to A.M.J. funded the biochemical aspects of this project. The content is solely
848 the responsibility of the authors and does not necessarily represent the official views of the
849 National Institutes of Health.

850

851 **AUTHOR CONTRIBUTIONS**

852 T.J.R-E., J.W., X.S., B.D., H.J., J.Y., M.T-O, F.L. and A.M.J. performed experiments and
853 produced data used in the figures. T.J.R-E., J.W., X.S., and A.M.J. designed experiments, and
854 analyzed results. P.K provided the MAPK reporters prior to its publication and guided those
855 experiments. L.W. synthesized and purified [^{14}C]isomaltulose. Y.T. performed sugar uptake
856 experiments shown in Figure 1. T.J.R-E., J.W., and A.M.J wrote the paper.

857 **DECLARATION OF INTERESTS**

858 The authors declare no competing interest.

859
860

861

862 **Figure legends**
863
864 **Figure 1. AtRGS1 perceives extracellular glucose or glucose metabolite**. While flg22 is
865 perceived extracellularly, an extracellular site of glucose perception for activation of G signaling
866 in Arabidopsis has not yet been made with an impermeant glucose analog. See supporting data
867 for this figure in Supplemental Material Figure S1. **A**. Isomaltulose and D-glucose induce rapid
868 AtRGS1-YFP endocytosis in a dose-dependent manner. Images are representative from hypocotyl
869 epidermal cells ectopically expressing AtRGS1 tagged with YFP. **B**. Despite being 9-fold less
870 permeant to the Arabidopsis plasma membrane, isomaltulose is slightly more potent than D-
871 glucose in activation of G signaling as measured by proxy using AtRGS1-YFP endocytosis (Fu et
872 al., 2014). **C**. Turanose is impermeant to plant cells (Rolland et al., 2002) yet is as effective as D-
873 glucose in inducing AtRGS1-YFP endocytosis. The purity of turanose was >98%. **D**. Structures.
874 Both isomaltulose and turanose share a glucose ring moiety.
875
876 **Figure 2. Two origins of AtRGS1 endocytosis.** Pharmacological inhibitors show two origins of
877 AtRGS1-YFP endocytosis. (**A**) AtRGS1-YFP seedlings were treated with increasing
878 concentrations of MβCD at 0mM (n= 18 (flg22) and 15 (glucose)), 1mM (n= 14 and 14), 2mM
879 (n= 15 and 16), 5mM (n= 17 and 14), 10mM (n= 12 and 17), and 20mM (n= 15 and 6) for 45 min
880 followed by incubation in the same solution but supplemented with 1 μM flg22 for 10 min or (**B**)
881 6% D-glucose for 30 min before imaging epidermal cells. Internalized AtRGS1-YFP was
882 quantified to determine total endocytosis of AtRGS1. MβCD does not inhibit flg22-induced
883 AtRGS1 endocytosis, but does partially inhibit glucose-induced AtRGS1 endocytosis at 5mM and
884 above ($p<0.01$). (**C**) TyrphostinA23, an inhibitor of CME, significantly impairs flg22-induced
885 AtRGS1 endocytosis (n=14) and (**D**) partially inhibits glucose-mediated AtRGS1 endocytosis

886 (n=27) ($p<0.01$). The structurally similar, but inactive analog of TyrA23, TyrA51, has no effect
887 (n=19) indicating the effect of TyrA23 is specific. (**E**) When both inhibitors are applied with
888 glucose, AtRGS1 internalization is reduced to basal levels (n=8) ($p<0.01$). A genetics approach to
889 inhibit AtRGS1 internalization confirms pharmacological results. (**F**) A genetic null mutant of
890 *ap2μ*, the cargo recognition complex for CME, results in complete inhibition of flg22-induced
891 AtRGS1 (n=16) ($p<0.01$) down to basal levels, confirming TyrA23 results. (**G**) Glucose-induced
892 internalization of AtRGS1 is partially inhibited in the *ap2μ* mutant (n=32) ($p<0.01$), but further
893 reduced to basal levels with the addition of MβCD (n=18) ($p<0.01$). (**H**) Mutation of Y^{112} to
894 Alanine in the AtRGS1 tyrosine motif recognized by ap2μ, $AtRGS1^{Y112A}$, inhibits flg22-induced
895 AtRGS1 endocytosis to basal levels (n=16) ($p<0.01$). (**I**) Glucose-mediated AtRGS1 endocytosis
896 is partially inhibited in $AtRGS1^{Y112A}$ (n=12) ($p<0.05$), but subsequently reduced to basal levels
897 with the addition of MβCD (n=9) ($p<0.01$). Quantification of AtRGS1-YFP fluorescence is
898 discussed in methods. (**J**) The speed and surface area of AtRGS1-GFP particles as tracked and
899 measured by IMARIS from 30 second time lapse imaging using TIRF at 5 minutes after treatment
900 with glucose and flg22. Identifiable AtRGS1-GFP particles are significantly smaller in the flg22
901 treated population (n=2026) compared to glucose (n=4619). No significant difference in speed is
902 observed between particles in the two treatments. (**K-P**) Endocytosis markers CLC-mCherry and
903 FLOT1-mCherry localize to the cell periphery and increase overlap with RGS1-GFP in a ligand
904 dependent manner after treatment with flg22 and glucose. Zeiss confocal micrographs show
905 AtRGS1-GFP (**green channel**) and either CLC-mCherry (**red channel K-M**) or FLOT1-mCherry
906 (**red channel N-P**) after 5 minute treatments with water (**K and N**), flg22 (**L and O**), and glucose
907 (**M and P**). After water treatment, CLC-mCherry (**K box inset**) and FLOT1-mCherry (**N box**
908 **inset**) remain distributed throughout the cell cytoplasm and highly overlapped AtRGS1-GFP

909 particles (**Q**). After treatment with flg22, CLC-mCherry migrates to the cell periphery with an
910 observed increase in protein agglomeration (**L red arrows**) and decrease overlap score with
911 RGS1GFP (**S**), while FLOT1-mCherry has no observable change compared to water (**G box inset**
912 **and R**). Upon treatment with glucose, FLOT1-mCherry protein bodies congregate at the cell
913 periphery (**P red arrows**) and decrease overlap with RGS1-GFP (**V**) , while CLC-mCherry
914 remains unchanged compared to water (**M box inset and U**). (**W**) The average overlap scores for
915 CLC-mCherry and FLOT1-mCherry after addition of water (n= 8 and 9), flg22 (n= 4 and 7), and
916 glucose (n= 4 and 3). flg22 addition induces a significant change in CLC compared to glucose and
917 water while glucose induces a significant change with FLOT1 compared to flg22 and water
918 ($p<0.01$).
919

920 **Figure 3. CME of AtRGS1 is phosphorylation dependent and G protein monomer specific.**
921 Known phosphorylation sites at serine residues on the C-terminal end of AtRGS1 are required for
922 both flg22 and glucose-induced CME of AtRGS1. (**A**) A truncated AtRGS1, AtRGS1$^{\Delta Ct}$, lacking
923 the 43 most C-terminal residues, including 8 serines, resulted in basal levels of flg22-induced
924 AtRGS1 internalization (n=11) ($p<0.01$). (**B**) Glucose-induced AtRGS1 internalization is partially
925 reduced in AtRGS1$^{\Delta Ct}$ (n=12) ($p<0.01$), but further reduced to basal levels with the addition of
926 MβCD (n=13) ($p<0.01$). (**C and D**) Mutation of three specific serine residues to alanine at 428,
927 435, and 436, in a full length AtRGS1, AtRGS1^{3SA}, yielded similar results to AtRGS1$^{\Delta Ct}$ for flg22
928 (n=10) and glucose-mediated internalization (n=22) ($p<0.01$), but indicate phosphorylation of one
929 or several specific serine residues is necessary for CME of AtRGS1. flg22 and glucose require
930 known kinases for AtRGS1 internalization. (**E**) Genetic ablation of the flg22 receptor FLS2 yields
931 basal levels of flg22-induced AtRGS1 internalization (n=12) ($p<0.01$), but does not affect glucose-

932 induced AtRGS1 internalization (n=9). (**F**) Similarly, null mutation of the BAK1 co-receptor,
933 *bak1-4*, results in ablated flg22-induced AtRGS1 internalization (n=16) ($p<0.01$), but not for
934 glucose (n=17) ($p=0.36$). (**G**) The high dose and low duration glucose specific WNK8 kinase is
935 necessary for glucose induced AtRGS1 internalization (n=13) ($p<0.01$), but not flg22 (n=10)
936 ($p=0.9$). Individual G proteins are necessary for AtRGS1 endocytosis in a ligand specific manner.
937 (**H**) A genetic null mutant of Gα, *gpa1-4*, limits flg22-induced endocytosis of AtRGS1 to basal
938 levels (n=15), while glucose-induced endocytosis is unaffected compared to wild-type (n=22). (**I**)
939 A null mutation of XLG2, *xlg2-1*, an extra-large Gα protein, also reduced flg22-induced AtRGS1
940 endocytosis to basal levels (n=14), but had no significant effect on glucose-mediated endocytosis
941 compared to wild type (n=19) ($p<0.01$). (**J**) A null mutation of the AGB1/AGG1 heterodimer,
942 *agb1-2/agg1*, inhibited flg22-induced AtRGS1 endocytosis (n=15), but had no effect on high dose,
943 low duration glucose-induced AtRGS1 endocytosis (n=17) ($p<0.01$). (**K**) At low dose, long
944 duration AGB1/AGG1 are necessary for glucose induced internalization (n=25). Quantification of
945 AtRGS1-YFP fluorescence is discussed in methods.
946
947 **Figure 4. Arabidopsis VPS26 subunits of the retromer complex may moonlight as arrestin-**
948 **like adaptors for AtRGS1 internalization**. (**A)** 3-D alignment of the model atvps26a-2 (colored
949 cyan) with the bovine arrestin-3 (PDB 3P2D, (colored wheat). The structure of model atvps26a-2
950 shows a similar arrestin scaffold with arrestin-3 which contains a semi-symmetric fold of two β
951 strand sandwich structures in the N domain and C domains linked by the central loops (ii); each
952 sandwich is formed by 3 or 4 β sheets, respectively. (**B)**. Differences between atvps26a-2 model
953 and bovine arrestin-3. Model atvps26a-2 lacks a short α-helix (i) inside the arrestin N-terminal
954 domain which has been implicated in receptor binding. Arrestin-3 contains a longer C terminal tail

955 which extend all the way to bind the N terminal domain which is important for clathrin-mediated
956 endocytosis (CME) in animals. The C terminus of atvps26a-2 has no extension. (**C**). The central
957 crest. The central crest of atvps26a is similar with that of arrestin-3 which includes the finger loop,
958 middle loop and the C loop, although arrestin-3 has a longer finger loop which is important for
959 receptor binding. (**D, E**) The polar core of bovine arrestin-3.The residues in the polar core of
960 arrestin-3 are Asp_{27}, Arg_{170}, Asp_{291}, Asp_{298} and Arg_{393} which are shown as vacuum electrostatics
961 (**D**) and sticks (**E**). (**F,G**) The polar core of atvps26A. The residues of atvps26a are the N domain
962 residues Glu_{118} and Tyr_{120}, and C domain residues Arg_{213}, Glu_{215}, Thr_{258}, Tyr_{272}, and Arg_{296} which
963 are also shown as vacuum electrostatics (**F**) and sticks (**G**). Although different amino acid
964 composition, both cores consist of similarly-positioned, positive-charged residues and allow the
965 formation of hydrogen bonds under physiological conditions. However, the orientation and shape
966 of the polar core of atvps26a-2 is distinct from arrestin-3. The arrestin-3 polar core is embedded
967 between β sheets in the N terminal domain whereas the atvps26a-2 core is open and elongated,
968 spanning the length of space between the N domain and C domain.
969
970 **Figure 5. Physical interaction between AtRGS1 and VPS26.** (**A**) Bifluorescence
971 complementation (BiFC) of VPS26A and VPS26B showing a specific head-to-tail orientation
972 requirement. Representative cells shown. n=5. Experiment repeated 2 times. (**B**) Split luciferase
973 complementation by VPS26A and VPS26B heterodimers and VPS26B homodimers. Error bars
974 are standard error of the mean (SEM). Means with different letters indicate significantly different
975 (Tukey's HSD test, $p<0.05$). n=64 leaf discs from 4 individual tobacco plants. (**C**) BiFC of VPS26
976 A and VPS26B with AtRGS1 in a specific orientation. (**D**) Split-luciferase complementation by
977 VPS26A and AtRGS1. Positive control is complementation by the heterotrimeric G protein

978 complex (GPA1/AGB1/AGG1). Negative control is AtGPA1 and AGB1 in the absence of AGG1.
979 Error bars are SEM. n=64. ($p<0.05$). (**E**) Yeast two-hybrid complementation between the
980 cytoplasmic domain of AtRGS1 (RGS1-J5) and VPS26B. RGS1-J5 contains the linker between
981 the 7TM domain and the RGS box, the RGS box and a C-terminal tail (CT). RGS1- ΔCT lacks the
982 C-terminal tail which contains the phosphorylation cluster required for AtRGS1 endocytosis.
983 RGS1- $\Delta CTS_{405,406A}$ lacks the CT and has two additional phosphosites mutated. –LW is the
984 leucine/tryptophan dropout, -LWH is the leucine/tryptophan/histidine drop out media; 10 mM 3-
985 AT indicates higher stringency by the addition of 10 mM 3-amino-1,2,4-triazole.

986

987 **Figure 6. MAPK activation and Ca^{2+} signaling in response to flg22 and D-glucose.** (**A-D**)
988 Processed confocal images of the epidermis of etiolated hypocotyls from the SOMA-NLS (**A, B**)
989 and SOMA-NES (**C, D**) transgenic lines depicting the ratio of YPet to Turquoise GL emission
990 produced by exciting Turquoise GL. Scale bar represents 100 µm. Time stamps indicate when the
991 image was collected labeled minutes:seconds. Images at 00:00 were collected before treatment,
992 while those at time point 20:00 were collected 5 minutes after treatment with 1 µM flg22. White
993 rectangle represent regions of interest (ROIs) used to measure YPet and Turquoise GL emission.
994 (**E-H**). The ratio of YPet to Turquoise GL emission produced by exciting Turquoise GL over time
995 was determined using the ROIs shown in (A-D). During the first 10 minutes of each experiment
996 the samples were incubated in water. The arrow indicates the time at which 1 µM flg22 (**E, G**) or
997 6% D-glucose (**F, H**) was added to the sample. (**E**) SOMA-NES lines pretreated with water
998 (orange) or 50 µM TyrA23 (yellow) prior to imaging. Inset graph (**F**) shows SOMA-NES line
999 pretreated with 6% D-glucose for 30 minutes prior to imaging. (**I**) flg22 dose-response in SOMA-
1000 NES lines. flg22 was added after two minutes of imaging. (**J, K**) R-GECO1 lines treated with

1001 flg22 or D-glucose in Col-0 (**J**) or *rgs1-2* (**K**) backgrounds. Fluorescence intensity changes of R-
1002 GECO1 in ~20 regions of interests in wild type plants. Fractional fluorescence changes (ΔF/F) for
1003 R-GECO1 were calculated from background corrected intensity values of R-GECO1 as (F −
1004 F0)/F0, where F0 represents the average fluorescence intensity of the baseline of a measurement
1005 of each genotype. Error bars are standard deviations. Asterisks represent statistical significance (*P*
1006 < 0.01) between treatment and water as determined by 2-way ANOVA.
1007
1008 **Figure 7. Component overview of flg22- and D-glucose-biased signaling. (A)** Simple model
1009 illustrating flg22 and glucose or metabolite input and the respective bias signaling output through
1010 AtRGS1, as well as a chart summary detailing the origins of endocytosis (CME and SDE),
1011 recognition motif and phosphorylation requirements, and individual proteins necessary for
1012 glucose- and flg22-induced endocytosis of AtRGS1. (**B**) Membrane overview illustrating proposed
1013 AtRGS1 microdomain clusters with common RLK neighbors. flg22 (orange circle) binds to FLS2
1014 to initiate signaling through AtRGS1. The mechanism of glucose (blue circle) perception is
1015 unknown as indicated by the question marks. After ligand perception, SDE or CME of AtRGS1
1016 occurs to permit downstream signaling. (**C**) A diagram of the individual components involved in
1017 the mechanism of endocytosis initiated by flg22 and glucose or metabolite. Numbers indicate the
1018 order of operations. For flg22: (1) perception of ligand, (2) phosphorylation of AtRGS1 by a RLK,
1019 (3 and 4) binding of clathrin complex and/or VPS26 in an unknown order, and (5) internalization
1020 of AtRGS1. For glucose or metabolite: (1) ligand perception by a RLK or direct interaction with
1021 AtRGS1, (2) receptor interaction with WNK kinase (in the case of SDE, #2 indicates immediate
1022 endocytosis because other key components of the pathway are unknown), (3) phosphorylation of
1023 AtRGS1 by WNK kinases, (4) binding of clathrin complex to AtRGS1, and (5) internalization of

1024 AtRGS1. TyrA23 is shown inhibiting CME in both pathways, while MβCD is shown inhibiting
1025 AtRGS1 microdomain formation at the membrane.
1026
1027 **Supplemental Information**
1028
1029
1030 **Supplemental Figure S1**. **Isomaltulose is nearly impermeant in Arabidopsis**. **A**. To test the
1031 permeability of Arabidopsis seedlings to isomaltulose, [^{14}C] isomaltulose was synthesized and
1032 purified to 84% as described in the methods. Sugar analysis is as described and the results shown.
1033 **B**. Uptake of [^{14}C] D-glucose and [^{14}C] isomaltulose into Arabidopsis seedlings was tested. AU,
1034 Arbitrary Units as described.
1035
1036 **Supplemental Figure S2. Tracking AtRGS1 after ligand addition.** (**A-E**) IMARIS surface
1037 tracking showing (**A**) the original wide-field image acquired by TIRF, (**B**) the tracked spots
1038 imposed on the original image and tracked at (**C**) 15s, (**D**) 30s, and (**F**) 60s after initiating time-
1039 lapse imaging. (**F-H**) Tracking results showing the (**F**) average speed and area for AtRGS1-GFP
1040 particles after addition of (**x**) flg22 and (**o**) glucose at 15 minutes post ligand addition. (**G**) area
1041 and (**H**) speed of AtRGS1-GFP particles are broken out into proportion of total tracked particles
1042 at 15 minutes post ligand addition. (**I-T**) Original field of view confocal micrographs highlighting
1043 areas used to calculate Manders Overlap Coefficients from Figure **2K-P** (white and yellow boxes)
1044 with the addition of 15 minute post ligand addition images.
1045

1046 **Supplemental Figure S3. G protein involvement in low dose, long duration sugar signaling**
1047 (**A**) 2% glucose addition for 6 hours to the genetic null mutant *wnk1-1* shows no discernable
1048 difference in AtRGS1 internalization compared to wild type (n=16) ($p<0.01$). (**B**) XLG2 is not
1049 necessary for AtRGS1 internalization with low-glucose DDR (n=18) ($p<0.01$).
1050
1051 **Figure S4. Supplemental data used to create the VPS26 model and comparison with arrestin**
1052 **structure described in main figure 4.** (**A**) Homogeneous sequence alignment of VPS26 family
1053 (Arabidopsis VPS26a, VPS26b, VPS26like and Human VPS26A, VPS26B) with arrestin family
1054 (Human arrestin-1, arrestin-2 and bovine arrestin-1, arrestin-2, arrestin-3, squid arrestin-1, shrimp
1055 arrestin-1)**.** (**B**) The identity matrix between arrestin family and VPS26 family. Clustal Omega
1056 https://www.ebi.ac.uk/Tools/msa/clustalo/ was used to generate the Multiple Sequence Alignment
1057 file and the identity matrix result. Then the ESPript 3.0 (Easy Sequencing in PostScript) which is
1058 a program which renders sequence similarities and secondary structure information from aligned
1059 sequences for analysis and publication purpose is used to generate the final alignment file
1060 http://espript.ibcp.fr/ESPript/ESPript/index.php. A percentage of equivalent residues is calculated
1061 per columns, considering physicochemical properties. A global score is calculated for all
1062 sequences by extracting all possible pairs of residues per columns, for the score greater than
1063 similarity GlobalScore (0.7), it was rendered as colored characters (red characters on a white
1064 background and white characters on a red background if residues are strictly conserved in the
1065 column) with blue frames. AtVPS26A has a high sequence identity of 91.06% with AtVPS26B
1066 and a 56.48% sequence identity with human VPS26A (shown in red box in figure B). AtVPS26A
1067 and the arrestin family share 14-20% sequence identity (shown in red box in the figure).
1068 Sequences: 1. DpArr1, squid arrestin-1; 2. p44, bovine arrestin-1 splice variant; 3. BtArr3, Bovine

1069 Arrestin-3; 4. PmArr1, shrimp arrestin-1; 5. BtArr1, Bovine Arrestin-1; 6. HsArr1, Human
1070 Arrestin-1; 7. BtArr2, Bovine Arrestin-2; 8. HsArr2, Human Arrestin-2; 9. AtVPS26like,
1071 Arabidopsis VPS26like; 10. AtVPS26A, Arabidopsis VPS26A; 11. AtVPS26B, Arabidopsis
1072 VPS26B; 12. HsVPS26A, human VPS26A; 13. BtVPS26A, bovine VPS26A; 14. HsVPS26B,
1073 human VPS26B; 15. BtVPS26B, bovine VPS26B.) (**C**) Model evaluation results of the 5 models
1074 of AtVPS26A. The MODELLER objective function (molpdf), DOPE assessment scores (Discrete
1075 Optimized Protein Energy, which is a statistical potential used to assess homology models in
1076 protein structure prediction), GA341 assessment score (range from 0.0 (worst) to 1.0 (native-like))
1077 and RMSD (root-mean-square deviation, Å) with the template were calculated to evaluate the
1078 models. The "best" model is selected with the lowest value of the molpdf, DOPE score and RMSD
1079 value. The second model (atvps26a-2) was selected given the best DOPE score and RMSD value.
1080 (**D**) DOPE per residue score files of the 5 atvps26a models and the template. DOPE per residue
1081 score files of the five atvps26a models and the template human VPS26A[2FAU] were plotted using
1082 GNUPLOT which is a portable command-line driven graphing utility http://www.gnuplot.info/.
1083 Upper panel is the curves of the five atvps26a models and the template. The lower panel is the
1084 curve of the "best" model atvps26a-2 with the template. (**E**) 3D-structural alignment
1085 between model atvps26a-2 with human VPS26a template (PDB [2FAU]). atvps26a-2 model
1086 colored in pale-cyan and human VPS26A template colored in bright-orange using pymol. Upper
1087 panel: Side view. Lower panel: Top view. (**F**) Etiolated hypocotyls of Col-0 and VPS26 null
1088 mutants at 5 days old, the age used for experiments in Figure 5. Seedlings were germinated and
1089 grown in liquid MS for 5 days and transferred to solid agar plates for imaging. Scale bar 5mm.
1090

1091 **Supplemental Figure S5. Positive and negative controls for SOMA markers.** (**A-D**) (**A**)
1092 Transgenic lines SOMA-NLS (Nuclear MAPK reporter) and (**B)** SOMA-NES (cytoplasmic
1093 MAPK reporter) were analyzed before and after treatment with 150 mM NaCl as a positive control
1094 and with water (**C** and **D**) as the negative control. (**E,F**) Negative control reporters: Mutants of
1095 the transgenic lines SOMA^{T679A}-NLS (**E**) and SOMA^{T679A}-NES (**F)** were treated with 1 µM flg22.
1096 (**G - O**) Replicate experimental tracings showing reproducibility of TyrA23 inhibition of the flg22-
1097 induced activation of G signaling via AtRGS1-YFP internalization (**G - N**) and its corresponding
1098 TyrA51 negative control (**O - V**). During the first 10 minutes of each experiment, SOMA-NES
1099 lines pretreated with 50 µM TyrA23 for 10 min (**G - N**) or 50 µM TyrA51 (**O - V**) for 30 minutes
1100 prior to activation with flg22. Each graph represents 1 individual hypocotyl and each trace is a
1101 region of interest. (**W**) SOMA-NES was pretreated with 6% D-glucose for 30 minutes prior to
1102 analysis. Hypocotyls were then treated with 1 µM flg22.
1103
1104 **Supplemental Figure S6. Positive and negative controls and dose response.** Transgenic lines
1105 SOMA-NLS and SOMA-NES were analyzed before and after treatment with 150 mM NaCl as a
1106 positive control (**A**, **B**) and water (**C**, **D**). (**E**, **F**) Mutants of the transgenic lines SOMA^{T679A}-NLS
1107 and SOMA^{T679A}-NES were treated with 1 µM flg22 during the first 10 minutes of each experiment
1108 the samples. SOMA-NES lines were pretreated with 50 µM TyrA23 (**G**-**N**) or 50 µM TyrA51 (**O**-
1109 **V**) for 30 minutes prior to imaging. (**W-AB**) flg22 dose-response in SOMA-NES lines. (**AC**-**AH**)
1110 flg22 dose-response in R-GECO1 lines. Each graph represents 1 individual hypocotyl.
1111
1112 **Supplemental Code. MatLab code for averaging unique tracked AtRGS1 particle speed and**
1113 **area.** Speed and area data from IMARIS is exported in xls format and imported to MatLab for

1114 sorting. Each AtRGS1 tracked protein or cluster has a unique trackID that is sorted while
1115 maintaining association with speed and area at defined time points. We identified the start and end
1116 location for each unique trackID and created a matrix to store the data and subsequently find the
1117 mean for speed and area within our defined time points.

1118

1119

1120 **REFERENCES**

1121

1122 Adam, T., Bouhidel, K., Der, C., Robert, F., Najid, A., Simon-Plas, F., and Leborgne-Castel, N.
1123 (2012). Constitutive expression of clathrin hub hinders elicitor-induced clathrin-mediated
1124 endocytosis and defense gene expression in plant cells. FEBS Letters *586*, 3293-3298.
1125

1126 Allen, J.A., Yost, J.M., Setola, V., Chen, X., Sassano, M.F., Chen, M., Peterson, S., Yadav, P.N.,
1127 Huang, X.-p., Feng, B.*, et al.* (2011). Discovery of β-arrestin–biased dopamine D_2 ligands for
1128 probing signal transduction pathways essential for antipsychotic efficacy. Proceedings of the
1129 National Academy of Sciences *108*, 18488-18493.
1130

1131 Alvarez, C.E. (2008). On the origins of arrestin and rhodopsin. BMC Evolutionary Biology *8*, 222.
1132

1133 Asai, T., Tena, G., Plotnikova, J., Willmann, M.R., Chiu, W.-L., Gomez-Gomez, L., Boller, T.,
1134 Ausubel, F.M., and Sheen, J. (2002). MAP kinase signalling cascade in Arabidopsis innate
1135 immunity. Nature *415*, 977-983.
1136

1137 Banbury, D.N., Oakley, J.D., Sessions, R.B., and Banting, G. (2003). Tyrphostin A23 inhibits
1138 internalization of the transferrin Receptor by perturbing the interaction between tyrosine motifs
1139 and the medium chain subunit of the AP-2 adaptor complex. J Biol Chem *278*, 12022-12028.
1140

1141 Bandyopadhyay, A., Van Eps, N., Eger, B.T., Rauscher, S., Yedidi, R.S., Moroni, T., West, G.M.,
1142 Robinson, K.A., Griffin, P.R., Mitchell, J.*, et al.* (2018). A novel polar core and weakly fixed C-
1143 tail in squid arrestin provide new insight into interaction with rhodopsin. Journal of Molecular
1144 Biology *430*, 4102-4118.
1145

1146 Bashline, L., Li, S., Anderson, C.T., Lei, L., and Gu, Y. (2013). The endocytosis of cellulose
1147 synthase in Arabidopsis Is dependent on μ2, a clathrin-mediated endocytosis adaptin. Plant
1148 Physiology *163*, 150-160.
1149

1150 Benovic, J., Kuhn, H., Weyand, I., Codina, J., Caron, M., and Lefkowitz, R. (1987). Functional
1151 desensitization of the isolated beta-adrenergic receptor by the beta-adrenergic receptor kinase:
1152 potential role of an analog of the retinal protein arrestin (48-kDa protein). Proceedings of the
1153 National Academy of Sciences of the United States of America *84*, 8879 - 8882.
1154

1155 Benovic, J.L., Strasser, R.H., Caron, M.G., and Lefkowitz, R.J. (1986). Beta-adrenergic receptor
1156 kinase: identification of a novel protein kinase that phosphorylates the agonist-occupied form of
1157 the receptor. Proceedings of the National Academy of Sciences *83*, 2797-2801.
1158

1159 Bohn, L.M., Gainetdinov, R.R., Lin, F.-T., Lefkowitz, R.J., and Caron, M.G. (2000). μ-Opioid
1160 receptor desensitization by β-arrestin-2 determines morphine tolerance but not dependence. Nature
1161 *408*, 720-723.
1162
1163

Börnke, F., Hajirezaei, M., Heineke, D., Melzer, M., Herbers, K., and Sonnewald, U. (2002). High-level production of the non-cariogenic sucrose isomer palatinose in transgenic tobacco plants strongly impairs development. Planta *214*, 356-364.

Boucrot, E., Saffarian, S., Zhang, R., and Kirchhausen, T. (2010). Roles of AP-2 in clathrin-mediated endocytosis. PLoS One *5*, e10597.

Butcher, A.J., Prihandoko, R., Kong, K.C., McWilliams, P., Edwards, J.M., Bottrill, A., Mistry, S., and Tobin, A.B. (2011). Differential G-protein-coupled receptor phosphorylation provides evidence for a signaling bar code. Journal of Biological Chemistry *286*, 11506-11518.

Charest, P.G., Oligny-Longpré, G., Bonin, H., Azzi, M., and Bouvier, M. (2007). The V2 vasopressin receptor stimulates ERK1/2 activity independently of heterotrimeric G protein signalling. Cellular Signalling *19*, 32-41.

Chen, J.-G., Willard, F.S., Huang, J., Liang, J., Chasse, S.A., Jones, A.M., and Siderovski, D.P. (2003). A seven-transmembrane RGS protein that modulates plant cell proliferation. Science *301*, 1728-1731.

Chen, L.-Q., Hou, B.-H., Lalonde, S., Takanaga, H., Hartung, M.L., Qu, X.-Q., Guo, W.-J., Kim, J.-G., Underwood, W., Chaudhuri, B.*, et al.* (2010). Sugar transporters for intercellular exchange and nutrition of pathogens. Nature *468*, 527.

Chen, Q., Iverson, T.M., and Gurevich, V.V. (2018). Structural basis of arrestin-dependent signal transduction. Trends in Biochemical Sciences *43*, 412-423.

Chen, Q., Zhuo, Y., Kim, M., Hanson, S.M., Francis, D.J., Vishnivetskiy, S.A., Altenbach, C., Klug, C.S., Hubbell, W.L., and Gurevich, V.V. (2014). Self-association of arrestin family members. In Arrestins - Pharmacology and Therapeutic Potential, V.V. Gurevich, ed. (Berlin, Heidelberg, Springer Berlin Heidelberg), pp. 205-223.

Chinchilla, D., Bauer, Z., Regenass, M., Boller, T., and Felix, G. (2006). The *Arabidopsis* receptor kinase FLS2 binds flg22 and determines the specificity of flagellin perception. The Plant Cell *18*, 465-476.

Choi, M., Staus, D.P., Wingler, L.M., Ahn, S., Pani, B., Capel, W.D., and Lefkowitz, R.J. (2018). G protein–coupled receptor kinases (GRKs) orchestrate biased agonism at the β₂-adrenergic receptor. Science Signaling *11*, eaar7084.

Collins, B.M., McCoy, A.J., Kent, H.M., Evans, P.R., and Owen, D.J. (2002). Molecular architecture and functional model of the endocytic AP2 complex. Cell *109*, 523-535.

DeFea, K.A., Zalevsky, J., Thoma, M.S., Déry, O., Mullins, R.D., and Bunnett, N.W. (2000). β-Arrestin–dependent endocytosis of proteinase-activated receptor 2 is required for intracellular targeting of activated Erk1/2. The Journal of Cell Biology *148*, 1267-1282.

1210 Delgado-Cerezo, M., Sánchez-Rodríguez, C., Escudero, V., Miedes, E., Fernández, P.V., Jordá,
1211 L., Hernández-Blanco, C., Sánchez-Vallet, A., Bednarek, P., Schulze-Lefert, P., *et al.* (2012).
1212 Arabidopsis heterotrimeric G-protein regulates cell wall defense and resistance to necrotrophic
1213 fungi. Molecular Plant *5*, 98-114.
1214
1215 DeWire, S.M., Yamashita, D.S., Rominger, D.H., Liu, G., Cowan, C.L., Graczyk, T.M., Chen, X.-
1216 T., Pitis, P.M., Gotchev, D., Yuan, C., *et al.* (2013). A G protein-biased ligand at the μ-opioid
1217 receptor is potently analgesic with reduced gastrointestinal and respiratory dysfunction compared
1218 with morphine. Journal of Pharmacology and Experimental Therapeutics *344*, 708-717.
1219
1220 Dhonukshe, P., Aniento, F., Hwang, I., Robinson, D.G., Mravec, J., Stierhof, Y.-D., and Friml, J.
1221 (2007). Clathrin-mediated constitutive endocytosis of PIN auxin efflux carriers in Arabidopsis.
1222 Current Biology *17*, 520-527.
1223
1224 Ding, L., Pandey, S., and Assmann, S.M. (2008). Arabidopsis extra-large G proteins (XLGs)
1225 regulate root morphogenesis. The Plant Journal *53*, 248-263.
1226
1227 Droillard, M.-J., Boudsocq, M., Barbier-Brygoo, H., and Lauriere, C. (2004). Involvement of
1228 MPK4 in osmotic stress response pathways in cell suspensions and plantlets of *Arabidopsis*
1229 *thaliana*: activation by hypoosmolarity and negative role in hyperosmolarity tolerance. FEBS
1230 Letters *574*, 42-48.
1231
1232 Eichel, K., and von Zastrow, M. (2018). Subcellular organization of GPCR signaling. Trends in
1233 Pharmacological Sciences *39*, 200-208.
1234
1235 Escudero, V., Jordá, L., Sopeña-Torres, S., Mélida, H., Miedes, E., Muñoz-Barrios, A., Swami, S.,
1236 Alexander, D., McKee, L.S., Sánchez-Vallet, A., *et al.* (2017). Alteration of cell wall xylan
1237 acetylation triggers defense responses that counterbalance the immune deficiencies of plants
1238 impaired in the β-subunit of the heterotrimeric G-protein. The Plant Journal *92*, 386-399.
1239
1240 Fan, L., Li, R., Pan, J., Ding, Z., and Lin, J. (2015). Endocytosis and its regulation in plants. Trends
1241 in Plant Science *20*, 388-397.
1242
1243 Felix, G., Duran, J.D., Volko, S., and Boller, T. (1999). Plants have a sensitive perception system
1244 for the most conserved domain of bacterial flagellin. The Plant Journal *18*, 265-276.
1245
1246 Ferguson, K.M., Higashijima, T., Smigel, M.D., and Gilman, A.G. (1986). The influence of bound
1247 GDP on the kinetics of guanine nucleotide binding to G proteins. J Biol Chem *261*, 7393-7399.
1248
1249 Fernie, A.R., Roessner, U., and Geigenberger, P. (2001). The sucrose analog palatinose leads to a
1250 stimulation of sucrose degradation and starch synthesis when supplied to discs of growing potato
1251 tubers. Plant Physiol *125*, 1967-1977.
1252
1253 Fu, Y., Lim, S., Urano, D., Tunc-Ozdemir, M., Phan, N., Elston, T., and Jones, A. (2014).
1254 Reciprocal encoding of signal intensity and duration in a glucose-sensing circuit. . Cell *156*, 1084-
1255 1096.

1256
1257 Géhin, M., Vivat, V., Wurtz, J.-M., Losson, R., Chambon, P., Moras, D., and Gronemeyer, H.
1258 (1999). Structural basis for engineering of retinoic acid receptor isotype-selective agonists and
1259 antagonists. Chemistry & Biology *6*, 519-529.
1260
1261 Gesty-Palmer, D., Chen, M., Reiter, E., Ahn, S., Nelson, C.D., Wang, S., Eckhardt, A.E., Cowan,
1262 C.L., Spurney, R.F., Luttrell, L.M.*, et al.* (2006). Distinct β-arrestin- and G protein-dependent
1263 pathways for parathyroid hormone receptor-stimulated ERK1/2 activation. Journal of Biological
1264 Chemistry *281*, 10856-10864.
1265
1266 Gómez-Gómez, L., and Boller, T. (2000). FLS2: An LRR receptor–like kinase involved in the
1267 perception of the bacterial elicitor flagellin in Arabidopsis. Molecular Cell *5*, 1003-1011.
1268
1269 Grigston, J.C., Osuna, D., Scheible, W.R., Stitt, M., and Jones, A.M. (2008). D-glucose sensing
1270 by a plasma membrane regulator of G signaling protein, AtRGS1. . FEBS Lett *582*, 3577-3584.
1271
1272 Gurevich, E., and Gurevich, V. (2006). Arrestins: ubiquitous regulators of cellular signaling
1273 pathways. Genome Biol *7*, 236.
1274
1275 Hao, H., Fan, L., Chen, T., Li, R., Li, X., He, Q., Botella, M.A., and Lin, J. (2014). Clathrin and
1276 membrane microdomains cooperatively regulate RbohD dynamics and activity in *Arabidopsis*.
1277 The Plant Cell *26*, 1729-1745.
1278
1279 Hirsch, J., Schubert, C., Gurevich, V., and Sigler, P. (1999). The 2.8 A crystal structure of visual
1280 arrestin: a model for arrestin's regulation. Cell *97*, 257 - 269.
1281
1282 Huot, B., Yao, J., Montgomery, B.L., and He, S.Y. (2014). Growth–defense tradeoffs in plants: A
1283 balancing act to optimize fitness. Molecular Plant *7*, 1267-1287.
1284
1285 Ilangumaran, S., and Hoessli, D.C. (1998). Effects of cholesterol depletion by cyclodextrin on the
1286 sphingolipid microdomains of the plasma membrane. Biochemical Journal *335*, 433-440.
1287
1288 Irani, N.G., Di Rubbo, S., Mylle, E., Van den Begin, J., Schneider-Pizoń, J., Hniliková, J., Šíša,
1289 M., Buyst, D., Vilarrasa-Blasi, J., Szatmári, A.-M.*, et al.* (2012). Fluorescent castasterone reveals
1290 BRI1 signaling from the plasma membrane. Nature chemical biology *8*, 583.
1291
1292 Jackson, L.P., Kelly, B.T., McCoy, A.J., Gaffry, T., James, L.C., Collins, B.M., Höning, S., Evans,
1293 P.R., and Owen, D.J. (2010). A large-scale conformational change couples membrane recruitment
1294 to cargo binding in the AP2 clathrin adaptor Complex. Cell *141*, 1220-1229.
1295
1296 Jelenska, J., Davern, S.M., Standaert, R.F., Mirzadeh, S., and Greenberg, J.T. (2017). Flagellin
1297 peptide flg22 gains access to long-distance trafficking in Arabidopsis via its receptor, FLS2.
1298 Journal of Experimental Botany *68*, 1769-1783.
1299
1300 Jha, S.G., Larson, E.R., Humble, J., Domozych, D.S., Barrington, D.S., and Tierney, M.L. (2018).
1301 Vacuolar Protein Sorting 26C encodes an evolutionarily conserved large retromer subunit in

1302 eukaryotes that is important for root hair growth in Arabidopsis thaliana. The Plant Journal *94*,
1303 595-611.
1304
1305 Johnston, C.A., Taylor, J.P., Gao, Y., Kimple, A.J., Grigston, J.C., Chen, J.-G., Siderovski, D.P.,
1306 Jones, A.M., and Willard, F.S. (2007). GTPase acceleration as the rate-limiting step in Arabidopsis
1307 G protein-coupled sugar signaling. Proceedings of the National Academy of Sciences *104*, 17317-
1308 17322.
1309
1310 Jones, J., Duffy, J., M, M., Temple, B., Dohlman, H., and Jones, A. (2011a). The crystal structure
1311 of a self-activating G protein α subunit reveals its distinct mechanism of signal initiation. Sci
1312 Signal *4*, ra8.
1313
1314 Jones, J.C., Temple, B.R.S., Jones, A.M., and Dohlman, H.G. (2011b). Functional reconstitution
1315 of an atypical G protein heterotrimer and regulator of G protein signaling protein (RGS1) from
1316 *Arabidopsis thaliana*. Journal of Biological Chemistry *286*, 13143-13150.
1317
1318 Kalderon, D., Roberts, B.L., Richardson, W.D., and Smith, A.E. (1984). A short amino acid
1319 sequence able to specify nuclear location. Cell *39*, 499-509.
1320
1321 Kang, Y., Zhou, X.E., Gao, X., He, Y., Liu, W., Ishchenko, A., Barty, A., White, T.A., Yefanov,
1322 O., Han, G.W.*, et al.* (2015). Crystal structure of rhodopsin bound to arrestin by femtosecond X-
1323 ray laser. Nature *523*, 561.
1324
1325 Keinath, N.F., Waadt, R., Brugman, R., Schroeder, Julian I., Grossmann, G., Schumacher, K., and
1326 Krebs, M. (2015). Live cell imaging with R-GECO1 sheds light on flg22- and chitin-induced
1327 transient $[Ca^{2+}]_{cyt}$ patterns in Arabidopsis. Molecular Plant *8*, 1188-1200.
1328
1329 Kelly, B.T., McCoy, A.J., Späte, K., Miller, S.E., Evans, P.R., Höning, S., and Owen, D.J. (2008).
1330 A structural explanation for the binding of endocytic dileucine motifs by the AP2 complex. Nature
1331 *456*, 976.
1332
1333 Kim, M., Vishnivetskiy, S.A., Van Eps, N., Alexander, N.S., Cleghorn, W.M., Zhan, X., Hanson,
1334 S.M., Morizumi, T., Ernst, O.P., Meiler, J.*, et al.* (2012). Conformation of receptor-bound visual
1335 arrestin. Proceedings of the National Academy of Sciences *109*, 18407-18412.
1336
1337 Kim, S.Y., Xu, Z.-Y., Song, K., Kim, D.H., Kang, H., Reichardt, I., Sohn, E.J., Friml, J., Juergens,
1338 G., and Hwang, I. (2013). Adaptor protein complex 2–mediated endocytosis is crucial for male
1339 reproductive organ development in *Arabidopsis*. The Plant Cell *25*, 2970-2985.
1340
1341 Klopffleisch, K., Phan, N., Augustin, K., Bayne, R.S., Booker, K.S., Botella, J.R., Carpita, N.C.,
1342 Carr, T., Chen, J.-G., Cooke, T.R.*, et al.* (2011). Arabidopsis G-protein interactome reveals
1343 connections to cell wall carbohydrates and morphogenesis. Mol Syst Biol *7*, 532.
1344
1345 Krauss, M., Kukhtina, V., Pechstein, A., and Haucke, V. (2006). Stimulation of
1346 phosphatidylinositol kinase type I-mediated phosphatidylinositol (4,5)-bisphosphate synthesis by
1347 AP-2μ–cargo complexes. Proceedings of the National Academy of Sciences *103*, 11934-11939.

1348
1349 Lee, J., Eschen-Lippold, L., Lassowskat, I., Böttcher, C., and Scheel, D. (2015). Cellular
1350 reprogramming through mitogen-activated protein kinases. Frontiers in Plant Science *6*.
1351
1352 Li, L., and Sheen, J. (2016). Dynamic and diverse sugar signaling. Current Opinion in Plant
1353 Biology *33*, 116-125.
1354
1355 Li, R., Liu, P., Wan, Y., Chen, T., Wang, Q., Mettbach, U., Baluška, F., Šamaj, J., Fang, X., Lucas,
1356 W.J.*, et al.* (2012). A membrane microdomain-associated protein, Arabidopsis Flot1, is involved
1357 in a clathrin-independent endocytic pathway and is required for seedling development. The Plant
1358 Cell *24*, 2105-2122.
1359
1360 Li, X., Wang, X., Yang, Y., Li, R., He, Q., Fang, X., Luu, D.-T., Maurel, C., and Lin, J. (2011).
1361 Single-molecule analysis of PIP2;1 dynamics and partitioning reveals multiple modes of
1362 Arabidopsis plasma membrane aquaporin regulation. The Plant Cell *23*, 3780-3797.
1363
1364 Liang, X., Ma, M., Zhou, Z., Wang, J., Yang, X., Rao, S., Bi, G., Li, L., Zhang, X., Chai, J.*, et al.*
1365 (2018). Ligand-triggered de-repression of Arabidopsis heterotrimeric G proteins coupled to
1366 immune receptor kinases. Cell Research.
1367
1368 Liao, K.-L., Melvin, C.E., Sozzani, R., Jones, R.D., Elston, T.C., and Jones, A.M. (2017). Dose-
1369 Duration Reciprocity for G protein activation: Modulation of kinase to substrate ratio alters cell
1370 signaling. PLoS ONE *12*, e0190000.
1371
1372 Lin, W.-W., and Hsieh, S.-L. (2011). Decoy receptor 3: A pleiotropic immunomodulator and
1373 biomarker for inflammatory diseases, autoimmune diseases and cancer. Biochemical
1374 Pharmacology *81*, 838-847.
1375
1376 Lin, Z.-J.D., Liebrand, T.W.H., Yadeta, K.A., and Coaker, G. (2015). PBL13 is a serine/threonine
1377 protein kinase that negatively regulates Arabidopsis immune responses. Plant Physiology *169*,
1378 2950-2962.
1379
1380 Lohse, M., Benovic, J., Codina, J., Caron, M., and Lefkowitz, R. (1990). beta-Arrestin: a protein
1381 that regulates beta-adrenergic receptor function. Science *248*, 1547 - 1550.
1382
1383 Loreti, E., Alpi, A., and Perata, P. (2000). Glucose and disaccharide-sensing mechanisms modulate
1384 the expression of alpha -amylase in barley embryos. Plant Physiol *123*, 939-948.
1385
1386 Luttrell, L.M., Roudabush, F.L., Choy, E.W., Miller, W.E., Field, M.E., Pierce, K.L., and
1387 Lefkowitz, R.J. (2001). Activation and targeting of extracellular signal-regulated kinases by β-
1388 arrestin scaffolds. Proceedings of the National Academy of Sciences *98*, 2449-2454.
1389
1390 Manglik, A., Lin, H., Aryal, D.K., McCorvy, J.D., Dengler, D., Corder, G., Levit, A., Kling, R.C.,
1391 Bernat, V., Hübner, H.*, et al.* (2016). Structure-based discovery of opioid analgesics with reduced
1392 side effects. Nature *537*, 185.
1393

1394 Martí-Renom, M.A., Stuart, A.C., Fiser, A., Sánchez, R., and, F.M., and Šali, A. (2000).
1395 Comparative protein structure modeling of genes and genomes. Annual Review of Biophysics and
1396 Biomolecular Structure *29*, 291-325.
1397
1398 Mudgil, Y., Karve, A., Teixeira, P., Jiang, K., Tunc-Ozdemir, M., and Jones, A. (2016).
1399 Photosynthate regulation of the root system architecture mediated by the heterotrimeric G protein
1400 complex in Arabidopsis. Frontiers in Plant Science *7*.
1401
1402 Nobles, K.N., Xiao, K., Ahn, S., Shukla, A.K., Lam, C.M., Rajagopal, S., Strachan, R.T., Huang,
1403 T.-Y., Bressler, E.A., Hara, M.R.*, et al.* (2011). Distinct phosphorylation sites on the β_2-adrenergic
1404 receptor establish a barcode that encodes differential functions of β-arrestin. Science Signaling *4*,
1405 ra51-ra51.
1406
1407 O'Hayre, M., Eichel, K., Avino, S., Zhao, X., Steffen, D.J., Feng, X., Kawakami, K., Aoki, J.,
1408 Messer, K., Sunahara, R.*, et al.* (2017). Genetic evidence that β-arrestins are dispensable for the
1409 initiation of β_2 adrenergic receptor signaling to ERK. Science Signaling *10*, eaal3395.
1410
1411 Ohno, H., Stewart, J., Fournier, M., Bosshart, H., Rhee, I., Miyatake, S., Saito, T., Gallusser, A.,
1412 Kirchhausen, T., and Bonifacino, J. (1995). Interaction of tyrosine-based sorting signals with
1413 clathrin-associated proteins. Science *269*, 1872-1875.
1414
1415 Ohtani, Y., Irie, T., Uekama, K., Fukunaga, K., and Pitha, J. (1989). Differential effects of alpha-
1416 , beta- and gamma-cyclodextrins on human erythrocytes. Eur J Biochem *186*, 17-22.
1417
1418 Oliviusson, P., Heinzerling, O., Hillmer, S., Hinz, G., Tse, Y.C., Jiang, L., and Robinson, D.G.
1419 (2006). Plant retromer, Localized to the prevacuolar compartment and microvesicles in
1420 *Arabidopsis*, may interact with vacuolar sorting receptors. The Plant Cell *18*, 1239-1252.
1421
1422 Paing, M.M., Stutts, A.B., Kohout, T.A., Lefkowitz, R.J., and Trejo, J. (2002). β-arrestins regulate
1423 protease-activated receptor-1 desensitization but not internalization or down-regulation. Journal of
1424 Biological Chemistry *277*, 1292-1300.
1425
1426 Pan, G., Ni, J., Wei, Y.-F., Yu, G.-l., Gentz, R., and Dixit, V.M. (1997). An antagonist decoy
1427 receptor and a death domain-containing receptor for TRAIL. Science *277*, 815-818.
1428
1429 Patwari, P., and Lee, R.T. (2012). An expanded family of arrestins regulate metabolism. Trends in
1430 Endocrinology & Metabolism *23*, 216-222.
1431 Peterson, Y.K., and Luttrell, L.M. (2017). The diverse roles of arrestin scaffolds in G protein–
1432 coupled receptor signaling. Pharmacological Reviews *69*, 256-297.
1433
1434 Pharr, D., and Keller, F. (2017). In Photoassimilate distribution plants and crops sSource-sink
1435 relationships (Routledge), pp. 157-183.
1436
1437 Raffaele, S., Bayer, E., Lafarge, D., Cluzet, S., German Retana, S., Boubekeur, T., Leborgne-
1438 Castel, N., Carde, J.-P., Lherminier, J., Noirot, E.*, et al.* (2009). Remorin, a solanaceae protein

1439 resident in membrane rafts and plasmodesmata, impairs potato virus X movement. The Plant Cell
1440 *21*, 1541-1555.
1441
1442 Rajagopal, S., Kim, J., Ahn, S., Craig, S., Lam, C.M., Gerard, N.P., Gerard, C., and Lefkowitz,
1443 R.J. (2010a). β-arrestin- but not G protein-mediated signaling by the "decoy" receptor CXCR7.
1444 Proceedings of the National Academy of Sciences *107*, 628-632.
1445
1446 Rajagopal, S., Rajagopal, K., and Lefkowitz, R.J. (2010b). Teaching old receptors new tricks:
1447 biasing seven-transmembrane receptors. Nature Reviews Drug Discovery *9*, 373.
1448
1449 Ranf, S., Eschen-Lippold, L., Pecher, P., Lee, J., and Scheel, D. (2011). Interplay between calcium
1450 signalling and early signalling elements during defence responses to microbe- or damage-
1451 associated molecular patterns. The Plant Journal *68*, 100-113.
1452
1453 Rives, M.-L., Rossillo, M., Liu-Chen, L.-Y., and Javitch, J.A. (2012). 6′-Guanidinonaltrindole (6′-
1454 GNTI) is a G protein-biased κ-opioid receptor agonist that inhibits arrestin recruitment. Journal
1455 of Biological Chemistry *287*, 27050-27054.
1456
1457 Rolland, F., Moore, B., and Sheen, J. (2002). Sugar sensing and signaling in plants. The Plant Cell
1458 *14*, S185-S205.
1459
1460 Schindelin, J., Arganda-Carreras, I., Frise, E., Kaynig, V., Longair, M., Pietzsch, T., Preibisch, S.,
1461 Rueden, C., Saalfeld, S., Schmid, B*., et al.* (2012). Fiji: an open-source platform for biological-
1462 image analysis. Nature Methods *9*, 676.
1463
1464 Shenoy, S.K., Drake, M.T., Nelson, C.D., Houtz, D.A., Xiao, K., Madabushi, S., Reiter, E.,
1465 Premont, R.T., Lichtarge, O., and Lefkowitz, R.J. (2006). β-Arrestin-dependent, G protein-
1466 independent ERK1/2 activation by the β2 adrenergic receptor. Journal of Biological Chemistry
1467 *281*, 1261-1273.
1468
1469 Shi, H., Rojas, R., Bonifacino, J.S., and Hurley, J.H. (2006). The retromer subunit Vps26 has an
1470 arrestin fold and binds Vps35 through its C-terminal domain. Nature Structural & Molecular
1471 Biology *13*, 540-548.
1472
1473 Shiraishi, Y., Natsume, M., Kofuku, Y., Imai, S., Nakata, K., Mizukoshi, T., Ueda, T., Iwaï, H.,
1474 and Shimada, I. (2018). Phosphorylation-induced conformation of β2-adrenoceptor related to
1475 arrestin recruitment revealed by NMR. Nature Communications *9*, 194.
1476
1477 Shiu, S.H., and Bleecker, A.B. (2001). Plant receptor-llike gene family: diversity, function, and
1478 signaling. Science STKE *Dec. 18th*, RE22.
1479
1480 Shukla, A.K., Manglik, A., Kruse, A.C., Xiao, K., Reis, R.I., Tseng, W.-C., Staus, D.P., Hilger,
1481 D., Uysal, S., Huang, L.-Y*., et al.* (2013). Structure of active β-arrestin-1 bound to a G-protein-
1482 coupled receptor phosphopeptide. Nature *497*, 137.
1483

1484 Sibley, D.R., Benovic, J.L., Caron, M.G., and Lefkowitz, R.J. (1987). Regulation of
1485 transmembrane signaling by receptor phosphorylation. Cell *48*, 913-922.
1486
1487 Sinha, A.K., Hofmann, M.G., Romer, U., Kockenberger, W., Elling, L., and Roitsch, T. (2002).
1488 Metabolizable and non-metabolizable sugars activate different signal transduction pathways in
1489 tomato. Plant Physiol *128*, 1480-1489.
1490
1491 Smith, J.S., Lefkowitz, R.J., and Rajagopal, S. (2018). Biased signalling: from simple switches to
1492 allosteric microprocessors. Nature Reviews Drug Discovery *17*, 243.
1493
1494 Smith, T.H., Coronel, L.J., Li, J.G., Dores, M.R., Nieman, M.T., and Trejo, J. (2016). Protease-
1495 activated receptor-4 signaling and trafficking is regulated by the clathrin adaptor protein complex-
1496 2 independent of β-arrestins. Journal of Biological Chemistry *291*, 18453-18464.
1497
1498 Sun, Y., Li, L., Macho, A.P., Han, Z., Hu, Z., Zipfel, C., Zhou, J.-M., and Chai, J. (2013). Structural
1499 basis for flg22-induced activation of the *Arabidopsis* FLS2-BAK1 immune complex. Science *342*,
1500 624-628.
1501
1502 Tunc-Ozdemir, M., and Jones, A.M. (2017). Ligand-induced dynamics of heterotrimeric G
1503 protein-coupled receptor-like kinase complexes. PLoS ONE *12*, e0171854.
1504
1505 Tunc-Ozdemir, M., Li, B., Jaiswal, D.K., Urano, D., Jones, A.M., and Torres, M.P. (2017).
1506 Predicted functional implications of phosphorylation of regulator of G protein signaling protein in
1507 plants. Frontiers in Plant Science *8*.
1508
1509 Tunc-Ozdemir, M., Liao, K.-L., Ross-Elliott, T.J., Elston, T.C., and Jones, A.M. (2018). Long-
1510 distance communication in Arabidopsis involving a self-activating G protein. Plant Direct *2*,
1511 e00037.
1512
1513 Tunc-Ozdemir, M., Urano, D., Jaiswal, D.K., Clouse, S.D., and Jones, A.M. (2016). Direct
1514 modulation of heterotrimeric G protein-coupled signaling by a receptor kinase complex. Journal
1515 of Biological Chemistry *291*, 13918-13925.
1516
1517 Urano, D., Maruta, N., Trusov, Y., Stoian, R., Liang, Y., Jaiswal, D., Thung, L., Botella, J., and
1518 Jones, A. (2016). Saltatory evolution of the heterotrimeric G protein signaling mechanisms in the
1519 plant kingdom. Science Signaling *9*, ra93.
1520
1521 Urano, D., Phan, N., Jones, J.C., Yang, J., Huang, J., Grigston, J., Philip Taylor, J., and Jones,
1522 A.M. (2012). Endocytosis of the seven-transmembrane RGS1 protein activates G-protein-coupled
1523 signalling in Arabidopsis. Nat Cell Biol *14*, 1079-1088.
1524
1525 Urs, N.M., Gee, S.M., Pack, T.F., McCorvy, J.D., Evron, T., Snyder, J.C., Yang, X., Rodriguiz,
1526 R.M., Borrelli, E., Wetsel, W.C.*, et al.* (2016). Distinct cortical and striatal actions of a β-arrestin–
1527 biased dopamine D2 receptor ligand reveal unique antipsychotic-like properties. Proceedings of
1528 the National Academy of Sciences *113*, E8178-E8186.
1529

1530 Urs, N.M., Peterson, S.M., and Caron, M.G. (2017). New concepts in dopamine D2 receptor biased
1531 signaling and implications for schizophrenia therapy. Biological Psychiatry *81*, 78-85.
1532
1533 Vang, S., Seitz, K., and Krysan, P. (2018). A simple microfluidic device for live cell imaging of
1534 Arabidopsis cotyledons, leaves, and seedlings. Biotechniques *64*, 255-261.
1535
1536 Vishnivetskiy, S.A., Gimenez, L.E., Francis, D.J., Hanson, S.M., Hubbell, W.L., Klug, C.S., and
1537 Gurevich, V.V. (2011). Few residues within an extensive binding interface drive receptor
1538 interaction and determine the specificity of arrestin proteins. Journal of Biological Chemistry *286*,
1539 24288-24299.
1540
1541 Vishnivetskiy, S.A., Paz, C.L., Schubert, C., Hirsch, J.A., Sigler, P.B., and Gurevich, V.V. (1999).
1542 How does arrestin respond to the phosphorylated state of rhodopsin? Journal of Biological
1543 Chemistry *274*, 11451-11454.
1544
1545 Wagemans, J., and Lavigne, R. (2015). Identification of protein-protein interactions by standard
1546 Gal4p-based yeast two-hybrid screening. In Protein-Protein Interactions: Methods and
1547 Applications, C.L. Meyerkord, and H. Fu, eds. (New York, NY, Springer New York), pp. 409-
1548 431.
1549
1550 Wen, W., Meinkotht, J.L., Tsien, R.Y., and Taylor, S.S. (1995). Identification of a signal for rapid
1551 export of proteins from the nucleus. Cell *82*, 463-473.
1552
1553 White, K.L., Robinson, J.E., Zhu, H., DiBerto, J.F., Polepally, P.R., Zjawiony, J.K., Nichols, D.E.,
1554 Malanga, C.J., and Roth, B.L. (2015). The G protein–biased opioid receptor agonist RB-64 is
1555 analgesic with a unique spectrum of activities *in vivo*. Journal of Pharmacology and Experimental
1556 Therapeutics *352*, 98-109.
1557
1558 Williams, L.E., Lemoine, R., and Sauer, N. (2000). Sugar transporters in higher plants – a diversity
1559 of roles and complex regulation. Trends in Plant Science *5*, 283-290.
1560
1561 Wingler, L.M., Elgeti, M., Hilger, D., Latorraca, N.R., Lerch, M.T., Staus, D.P., Dror, R.O.,
1562 Kobilka, B.K., Hubbell, W.L., and Lefkowitz, R.J. (2019). Angiotensin analogs with divergent
1563 bias stabilize distinct receptor conformations. Cell *176*, 468-478.e411.
1564
1565 Wu, L., and Birch, R. (2011). Isomaltulose is actively metabolized in plant cells. Plant Physiol
1566 *157*, 2094-2101.
1567
1568 Yang, F., Yu, X., Liu, C., Qu, C.-X., Gong, Z., Liu, H.-D., Li, F.-H., Wang, H.-M., He, D.-F., Yi,
1569 F.*, et al.* (2015). Phospho-selective mechanisms of arrestin conformations and functions revealed
1570 by unnatural amino acid incorporation and 19F-NMR. Nature Communications *6*, 8202.
1571
1572 Yang, Z., Yang, F., Zhang, D., Liu, Z., Lin, A., Liu, C., Xiao, P., Yu, X., and Sun, J.-P. (2017).
1573 Phosphorylation of G protein-coupled receptors: from the barcode hypothesis to the flute model.
1574 Molecular pharmacology *92*, 201-210.
1575

1576 Zaman, N., Seitz, K., Kabir, M., George-Schreder, L.S., Shepstone, I., Liu, Y., Zhang, S., and
1577 Krysan, P.J. (2019). A Förster resonance energy transfer sensor for live-cell imaging of mitogen-
1578 activated protein kinase activity in Arabidopsis. The Plant Journal *97*, 970-983.
1579
1580 Zelazny, E., Santambrogio, M., Pourcher, M., Chambrier, P., Berne-Dedieu, A., Fobis-Loisy, I.,
1581 Miège, C., Jaillais, Y., and Gaude, T. (2013). Mechanisms governing the endosomal membrane
1582 recruitment of the core retromer in Arabidopsis. Journal of Biological Chemistry *288*, 8815-8825.
1583
1584 Zhan, X., Gimenez, L.E., Gurevich, V.V., and Spiller, B.W. (2011). Crystal structure of arrestin-
1585 3 reveals the basis of the difference in receptor binding between two non-visual subtypes. Journal
1586 of Molecular Biology *406*, 467-478.
1587
1588 Zhong, C.-L., Zhang, C., and Liu, J.-Z. (2018). Heterotrimeric G protein signaling in plant
1589 immunity. Journal of Experimental Botany *70*, 1109-1118.
1590
1591 Zhou, Z., Bi, G., and Zhou, J.-M. (2018). Luciferase complementation assay for protein-protein
1592 interactions in plants. Current Protocols in Plant Biology *3*, 42-50.
1593
1594
1595
1596
1597
1598
1599
1600
1601
1602
1603
1604
1605

1606 Figure 1
1607

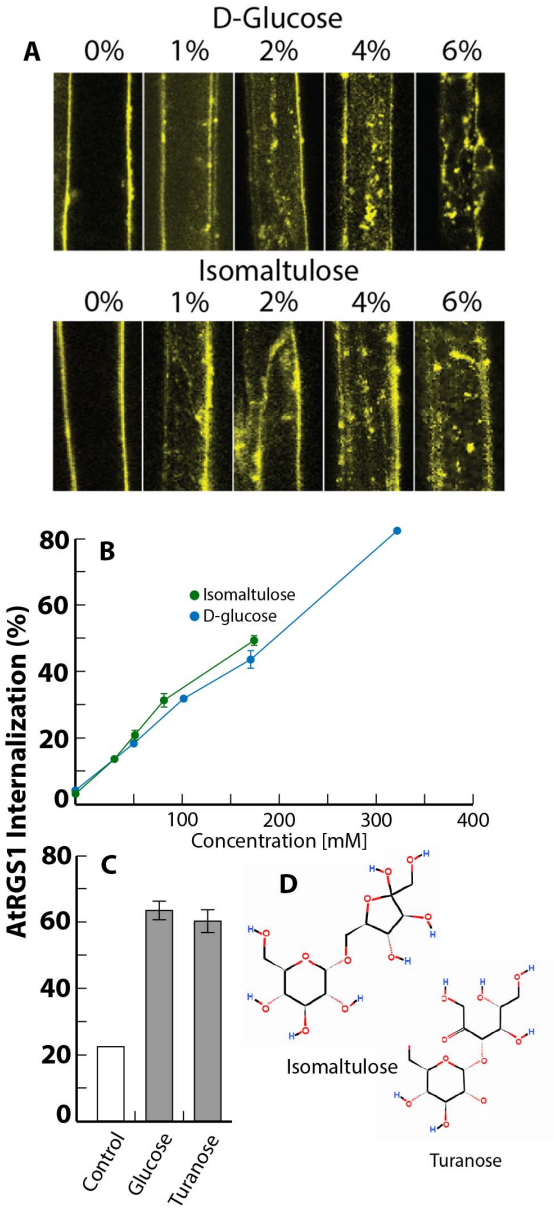

1608
1609
1610
1611
1612
1613
1614
1615

1616 Figure 2
1617

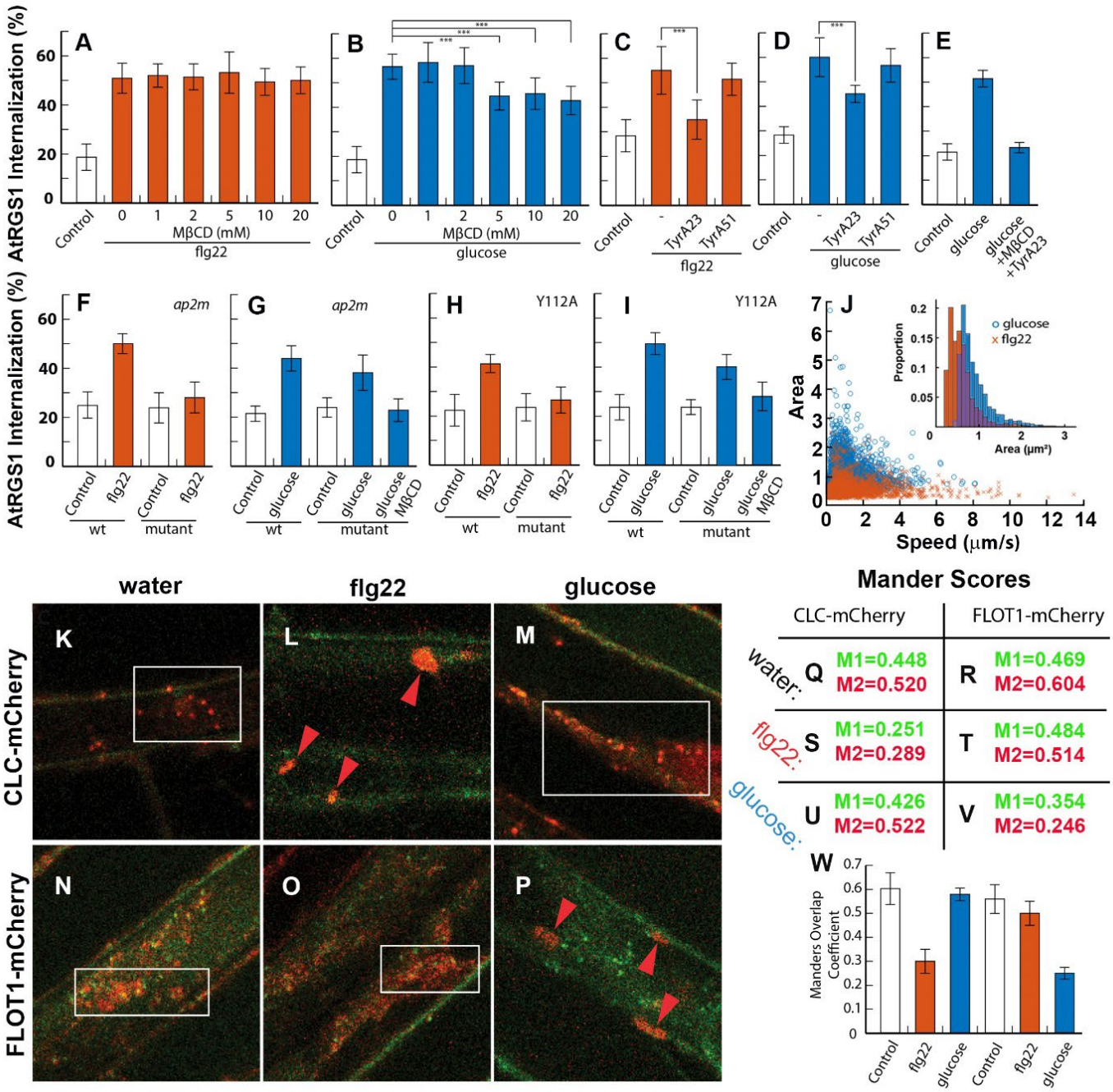

1618
1619
1620
1621
1622
1623
1624
1625

1626 Figure 3
1627

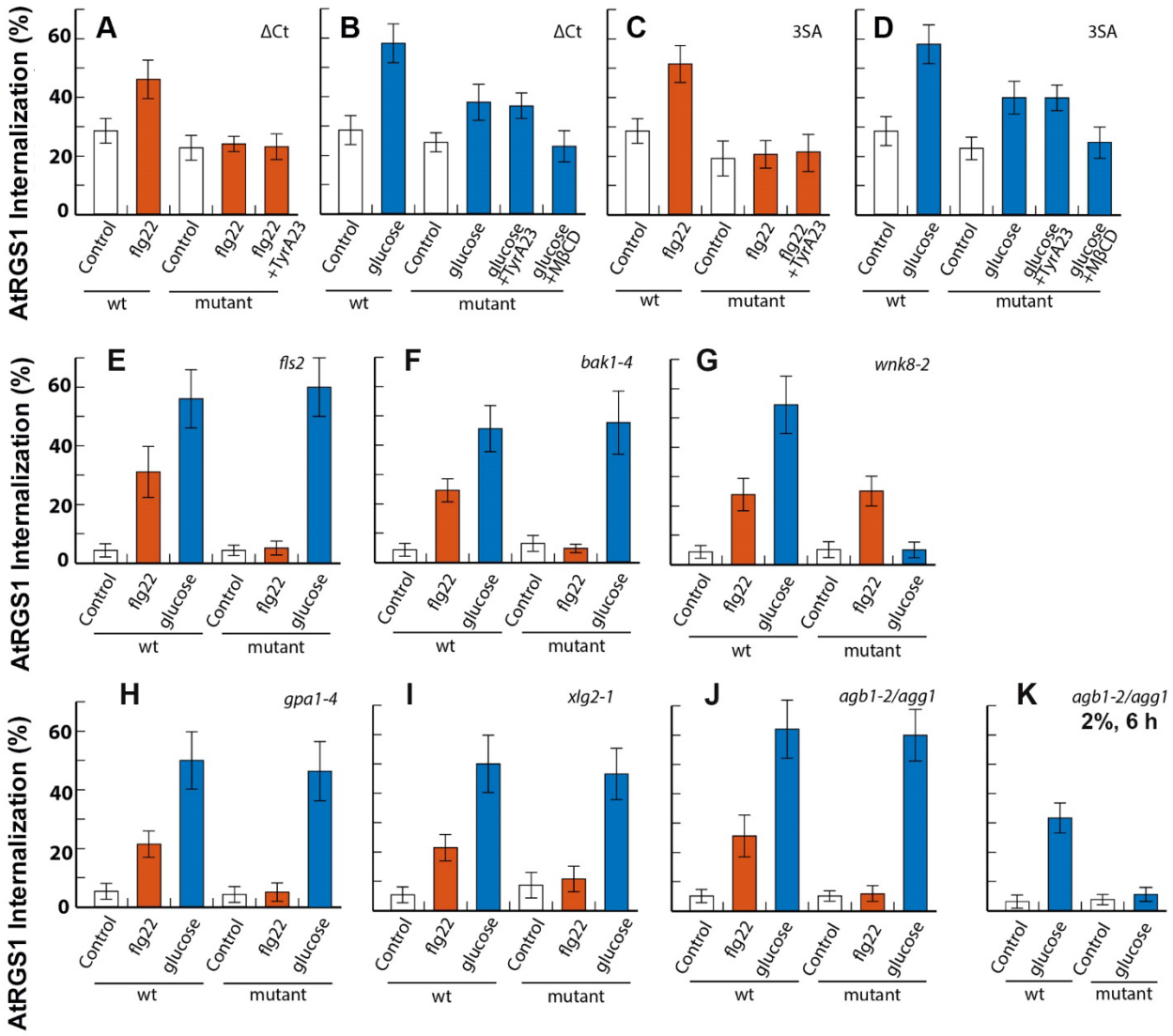

1628
1629
1630
1631
1632
1633
1634
1635
1636
1637
1638
1639
1640
1641
1642

1643 Figure 4
1644

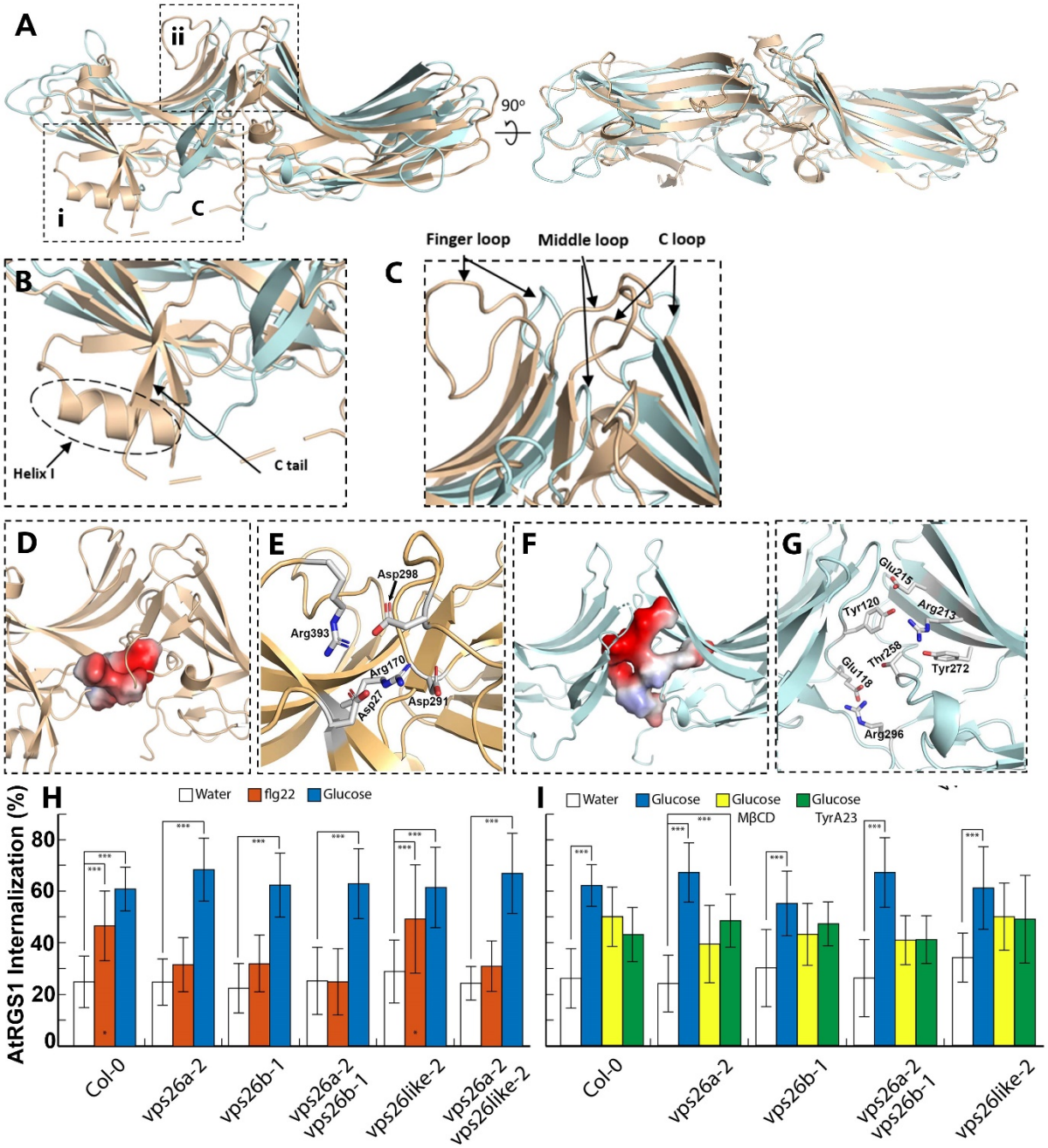

1645
1646
1647
1648
1649
1650
1651
1652

1653 Figure 5
1654

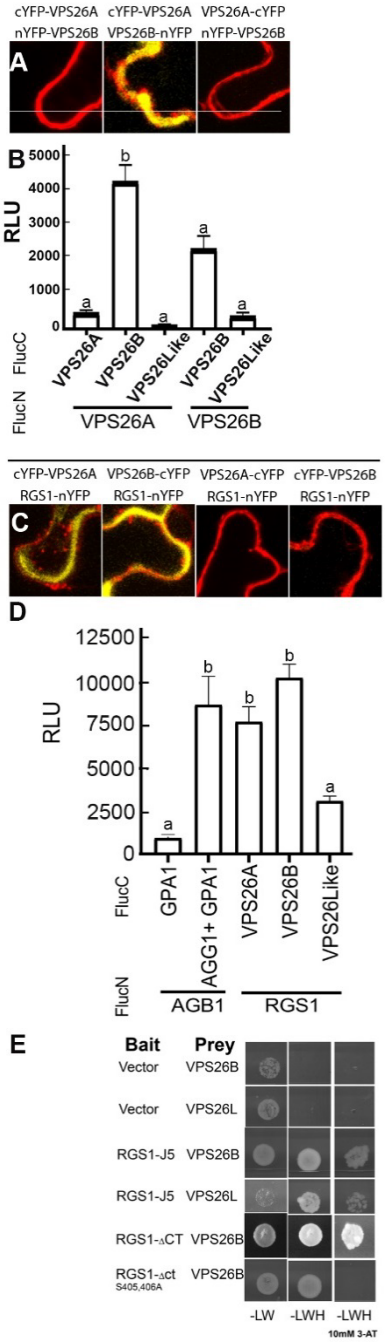

1655
1656
1657
1658
1659
1660
1661
1662

1663 Figure 6
1664

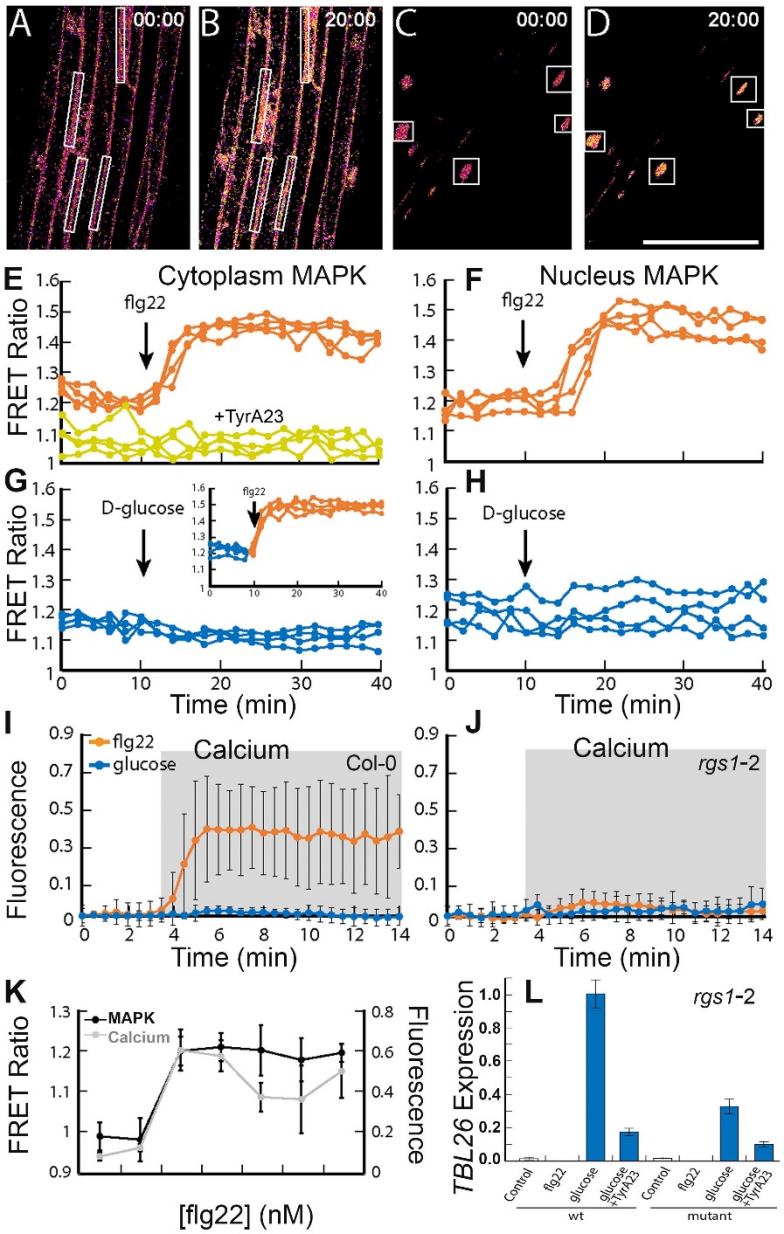

1665
1666
1667
1668
1669
1670
1671
1672
1673
1674
1675

1676 Figure 7

1677

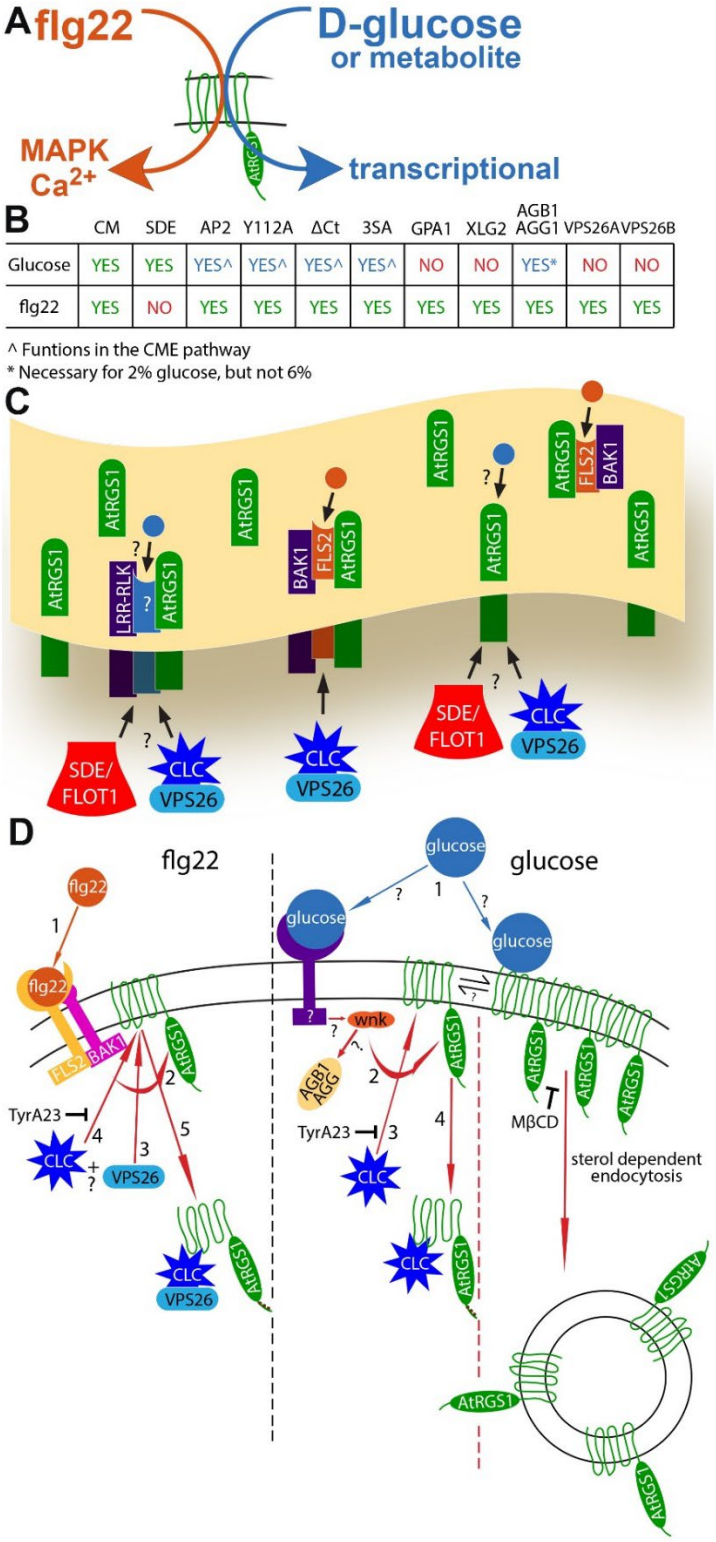

1678

1679

1680 Figure S1
1681

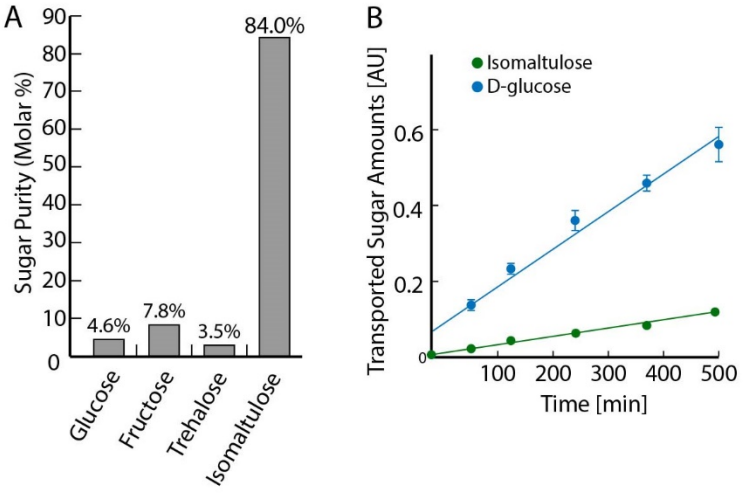

1682
1683
1684
1685
1686
1687
1688
1689
1690
1691
1692
1693
1694
1695
1696
1697
1698
1699
1700
1701
1702
1703
1704
1705
1706
1707
1708
1709
1710
1711
1712
1713

1714 Figure S2

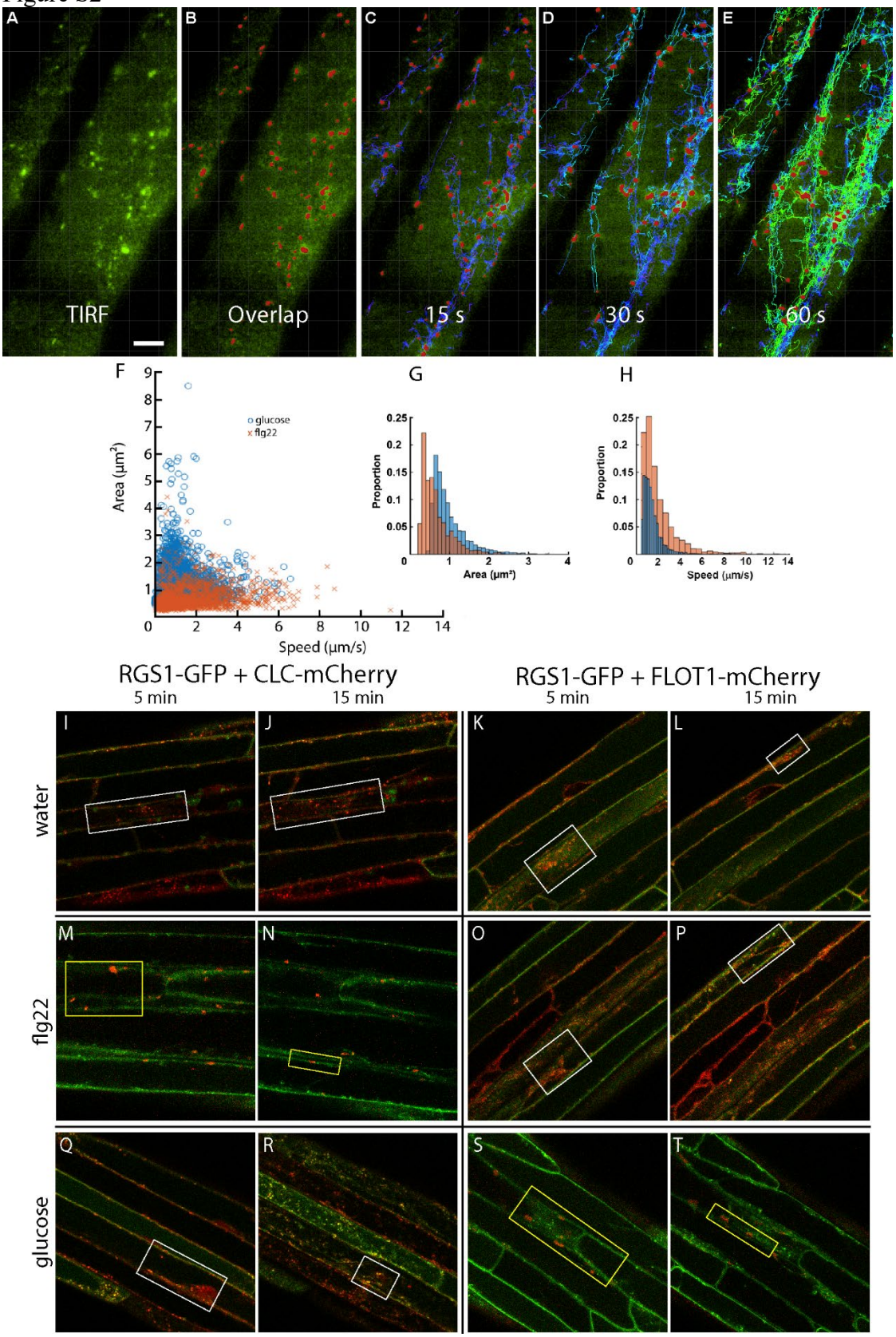

1715

1716 Figure S3
1717

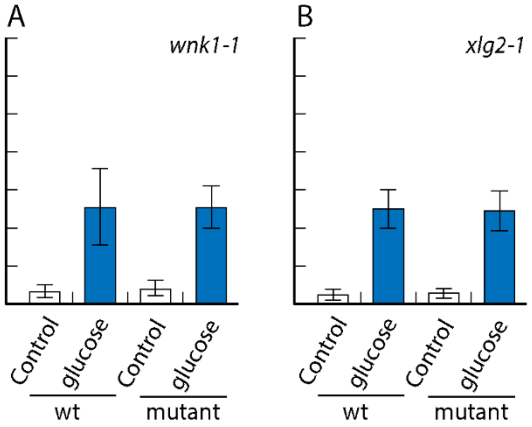

1718
1719
1720
1721
1722
1723
1724
1725
1726
1727
1728
1729
1730
1731
1732
1733
1734
1735
1736
1737
1738
1739
1740
1741
1742
1743
1744
1745
1746
1747
1748
1749
1750
1751

Figure S4

A

```
                 1        10        20        30        40        50        60        70
DpArr1      ...MGSWSHPQFEKGMV...TKKAKVYKKASPNGKLTTYLAKRDYYDHKEWQDNIDGVCVVDPDYLKNRKVFGLIVVAFRYG
p44         ...........MKANKP...APNHVIFKKISRDKSVTIYLGKRDYIDHVERVEPVDGVVLVDPELVKGKRVYVSLTCAFRYG
BtArr3      ................M...ANMSRVFKKTCSNGKLSIYLGKRDFVDHVDMVEPIDGVVLVDPEYLKGRKMFVMLTCAFRYG
PmArr1      ...........MEDNSK...RQGTRVFKKSSPNGKITVYLGKRDFVDHITHVDPIDGVVLIDPEYLKDRKVFGHVLAAFRYG
BtArr1      ...............MG...DKGTRVFKKASPNGKLTVYLGKRDFVDHIDLVEPVDGVVLVDPEYLKERRVYVTLTCAFRYG
HsArr1      ...............MG...DKGTRVFKKASPNGKLTVYLGKRDFVDHIDLVDPVDGVVLVDPEYLKERRVYVTLTCAFRYG
BtArr2      ..............MGE...KPGTRVFKKSSPNCKLTVYLGKRDFVDHLDKVDPVDGVVLVDPDYLKDRKVFVTLTCAFRYG
HsArr2      ..............MGE...KPGTRVFKKSSPNCKLTVYLGKRDFVDHLDKVDPV...............VFVTLTCAFRYG
AtVPS26like ..........................MATATTVNVKLS......RSNRIYRSSEPVEGKIVIK...SATSISHQAIRLSV.NG
AtVPS26A    MNYLLGAFKPACNISITFTDGKNRKQVPTKKDNGQ.I......VMNPLFQSQETIAGKINIEP.YQGKKVEHNGVKVEL.LG
AtVPS26B    MNYLLGAFKPACNISITFSDGKNRKQVPMKKENGQ.T......ALVPLFHSQDTISGKVCIEP.YQGKKVEHNGVKVEL.LG
HsVPS26A    MSFLGGFFGPICEIDIVLNDGETRKMAEMKTEDGK.V......EKHYLFYDGESVSGKVNLAFKQPGKRLEHQGIRIEF.VG
BtVPS26A    MSFLGGFFGPICEIDVVLNDGETRKMAEMKTEDGK.V......EKHYLFYDGESVSGKVNLAFKQPGKRLEHQGIRIEF.VG
HsVPS26B    MSFFG..FGQSVEVEILLNDAESRKRAEHKTEDGK.K......EKYFLFYDGETVSGKVSLALKNPNKRLEHQGIKIEF.IG
BtVPS26B    MSFFG..FGQSVDVDILLNDADSRRRAEHKTEDGK.K......DKYFLFYDGETVSGKVSLALKNPNKRLEHQGIKVEF.IG

                80        90       100       110       120       130       140       150
DpArr1      REDMDVMGVSFR..KDFA..VKQMQIYPPLEEN.QRPLTKLQAKLLNKLGENAVPFHYDLPTNTPDTVCIQPSEYDGGAPCG
p44         QEDIDVMGLSFR..RDLY..FSQVQVFPPVGA..SGATTRLQESLIKKLGANTYPFLLTFPDYLPCSVMLQPAPQDVGKSCG
BtArr3      HDDLDVIGLTFR..KDLY..VQVQQVVPAESSSPRGSLTVLQERLLHKLGDNAYPFTLQMVVNLPCSVTLQPGPDDTGKACG
PmArr1      REDLDVLGLTFR..KDLY..LASEQIFPLDPNN.KRPLTRLQERLIKKLGPNAFPFFFELPPHCPASVTLQPAPGDMGKPCG
BtArr1      REDLDVLGLTFR..KDLF..VANVQSFPPAPED.KKPLTRLQERLIKKLGEHAYPFTFEIPPNLPCSVTLQPGPEDTGKACG
HsArr1      REDLDVLGLTFR..KDLF..VANVQSFPPAPED.KKPLTRLQERLIKKLGEHAYPFTFEIPPNLPCSVTLQPGPEDTGKACG
BtArr2      REDLDVLGLSFR..KDLF..IANYQAFPPTPNP.PRPPTRLQERLLRKLGQHAHPFFFTIPQNLPCSVTLQPGPEDTGKACG
HsArr2      REDLDVLGLSFR..KDLF..IATYQAFPPVPNP.PRPPTRLQDRLLRKLGQHAHPFFFTIPQNLPCSVTLQPGPEDTGKACG
AtVPS26like SVNLQVRGGSAGVIESFYGVIKPIQIVKKTIE........VKSSGKIPPGTTEIPFSLNLREPGEGIV.EKFYETFHGTNIN
AtVPS26A    QIEMYFDRGNFY...DFTSLVR.........E........IDVPGEIYER.KTYPF.......EFSSV.EMPYETYNGVNVR
AtVPS26B    QIEMYFDRGNFY...DFTSLVR.........E........LDVPGEIYER.KTYPF.......EFPTV.EMPYETYNGVNVR
HsVPS26A    QIELFNDKSNTH...EFVNLVK.........E........LALPGELTQS.RSYDF.......EFMQV.EKPYESYIGANVR
BtVPS26A    QIELFNDKSNTH...EFVNLVK.........E........LALPGELTQS.RSYDF.......EFMQV.EKPYESYIGANVR
HsVPS26B    QIELYYDRGNHH...EFVSLVK.........D........LARPGEITQS.QAFDF.......EFTHV.EKPYESYTGQNVK
BtVPS26B    QIELYYDRGNHH...EFVSLVK.........D........LARPGEVTQS.QAFDF.......EFTHV.EKPYESYTGQNVK

               160       170                 180                 190       200                 210
DpArr1      VDYQVTTYVSQN...MDDKIH........KRNSVSLSIR......KLSYFEFGSDEQPRGEISKE..FK...FTSGAMKLEC
p44         VDFEIKAFATHSTDVEEDKIP........KKSSVRLLIR......KVQHAPRDMGPQPRAEASWQ..FF...MSDKPLRLAV
BtArr3      VDFEVKSFCAEN...LEEKVS........KRDSVRLVIR......KIQFAPLEPGPGPWARLCRR..FL...LSAQPLLLQA
PmArr1      VDYELKAYVGDT...VDDKPH........KRNSVRLAIR......KVMYAPIKQGEQPSVEVSKE..FM...MSPNKLHLEA
BtArr1      VDYEVKAFCAEN...LEEKIH........KRNSVRLVIR......KVQYAPERPGPQPTAETTRQ..FL...MSDKPLHLEA
HsArr1      VDYEVKAFCAEN...LEEKIH........KRNSVRLVIR......KVQYAPERPGPQPTAETTRQ..FL...MSDKPLHLEA
BtArr2      VDFEIRAFCAKS...LEEKSH........KRNSVRLVIR......KVQFAPEKPGPQPSAETTRH..FL...MSDRSLHLEA
HsArr2      VDFEIRAFCAKS...LEEKSH........KRNSVRLVIR......KVQFAPEKPGPQPSAETTRH..FL...MSDRSLHLEA
AtVPS26like IQYLLTADIPRG...YLHKPLSATMEFIIESGRVDLPERPIPPEIVIFYITQDTQRHPLLPDIKTGGFRVTGKLATQCSLQD
AtVPS26A    LRYVLKVTVTRG...YAGSIVEY.QDFVV.RNYVPLPPIN..NSIKME.V........GIEDCLHIEFE...YNKSKYHLKD
AtVPS26B    LRYVLKVTVTRG...YAGSILEY.QELVV.RNYAPLPDIN..NSIKME.V........GIEDCLHIEFE...YNKSKYHLKD
HsVPS26A    LRYFLKVTIVRR...LTDLVKEY..DLIV.HQLATYPDVN..NSIKME.V........GIEDCLHIEFE...YNKSKYHLKD
BtVPS26A    LRYFLKVTIVRR...LTDLVKEY..DLIV.HQLATYPDVN..NSIKME.V........GIEDCLHIEFE...YNKSKYHLKD
HsVPS26B    LRYFLRATISRR...LNDVVKEM..DIVV.HTLSTYPELN..SSIKME.V........GIEDCLHIEFE...YNKSKYHLKD
BtVPS26B    LRYFLRATISRR...LNDVVKEM..DIVV.HTLSTYPELN..SSIKME.V........GIEDCLHIEFE...YNKSKYHLKD

               220       230       240       250       260       270       280       290
DpArr1      TLDKARYYSGESMNISVCVDNPTSKKAKRIKIQIIQLADICLYETVTYKSVVTELETEEGFPIEPNTSGFCQVYKLRPVLEV
p44         SLSKEIYYHGEPIPVTVAVTNSTEKTVKKIKVLVEQVTNVVLYSSDYYIKTVAAEEAQE..KVPPN.SSLTKTLTLVPLLAN
BtArr3      WMDKEVNYHGQPISVNVSINNSTNKVIKKIKISVDQITDVVLYSLDKYTKTVFVQEFTE..TIAAN.STFSKSFAVTPLLAD
PmArr1      SLDKELYYHGETVAVNVHIQNNSNKSVKKIKVSIRQFADICLFSTAQYKCTVAETESEEGCPVGPG.FSISKVFTLTPLLSN
BtArr1      SLDKEIYYHGEPISVNVHVTNNTNKTVKKIKISVRQYADICLFNTAQYKCPVAMEEADD..TVAPS.STFCKVYTLTPFLAN
HsArr1      SLDKEIYYHGEPISVNVHVTNNTNKTVKKIKISVRQYADICLFNTAQYKCPVAMEEADD..TVAPS.STFCKVYTLTPFLAN
BtArr2      SLDKELYYHGEPLNVNVHVTNNSTKTVKKIKVSVRQYADICLFSTAQYKCPVAQVEQDD..QVSPS.STFCKVYTITPLLSN
HsArr2      SLDKELYYHGEPLNVNVHVTNNSTKTVKKIKVSVRQYADICLFSTAQYKCPVAQLEQDD..QVSPS.STFCKVYTITPLLSD
AtVPS26like PLSGELTVEASSVPI............TSIDIHLLRVE.....................................
AtVPS26A    VILGKIYFLLVRIKI............KNMDLEIRRRE.....................................
AtVPS26B    VILGKIYFLLVRIKM............KNMDLEIRRRE.....................................
HsVPS26A    VIVGKIYFLLVRIKI............QHMELQLIKKE.....................................
BtVPS26A    VIVGKIYFLLVRIKI............QHMELQLIKKE.....................................
HsVPS26B    VIVGKIYFLLVRIKI............KHMEIDIIKRE.....................................
BtVPS26B    VIVGKIYFLLVRIKI............KHMEIDIIKRE.....................................
```

```
                290       300       310       320       330                                340
DpArr1          KLRPVLEVTKRRAGLALNGKVKYEDTMLAASTEDAGNVDKENLGVV....................VSYKVRIKMTLGFG
p44             TLVPLLANNRERRGIALDGKIKHEDTNLASSTIIKEGIDKTVMGIL....................VSYQIKVKLTV..S
BtArr3          AVTPLLADNCHKQGLALDGKLKQGDTNLASSTILRPGVDKELLGIL....................VSYKVRVNLMVSCE
PmArr1          TLTPLLSNNRDKWGLALDGKLKDEDTNLASSTVITDSSQKENLGII....................VQYKVKVKLNL..G
BtArr1          TLTPFLANNREKRGLALDGKLKHEDTNLASSTLLREGANREILGII....................VSYKVKVKLVVSRG
HsArr1          TLTPFLANNREKRGLALDGKLKHEDTNLASSTLLREGANREILGII....................VSYKVKVKLVVSRG
BtArr2          TITPLLSNNREKRGLALDGKLKHEDTNLASSTIVKEGANKEVLGIL....................VSYRVKVKLVVSRG
HsArr2          TITPLLSDNREKRGLALDGKLKHEDTNLASSTIVKEGANKEVLGIL....................VSYRVKVKLVVSRG
AtVPS26like     ...............SIIVGERIVTETSLIQSTQIADGDVCRNMTLPIYVLLPRLLMCPSVF..AGPFSVEFKVCITISFK
AtVPS26A        ...............STGAGANTHVETETLAKFELMDGAPVRGESIPVRVFLTPYDLTPTHKNINNKFSVKYYLNLVLVDE
AtVPS26B        ...............STGAGANTHVETETLAKFELMDGTPVRGESIPVRLFLAPYDLTPTHRNINNKFSVKYYLNLVLVDE
HsVPS26A        ...............ITGIGPSTTTETETIAKYEIMDGAPVKGESIPIRLFLAGYDPTPTMRDVNKKFSVRYFLNLVLVDE
BtVPS26A        ...............ITGIGPSTTTETETIAKYEIMDGAPVKGESIPIRLFLAGYDPTPTMRDVNKKFSVRYFLNLVLVDE
HsVPS26B        ...............TTGTGPNVYHENDTIAKYEIMDGAPVRGESIPIRLFLAGYELTPTMRDINKKFSVRYYLNLVLIDE
BtVPS26B        ...............TTGTGPNVYHENDTIAKYEIMDGAPVRGESIPIRLFLAGYELTPTMRDINKKFSVRYYLNLVLIDD

                     350       360       370       380
DpArr1          .......SGDMLLEVPFKLCPARLKGRLAQPEARE.GDDAE.........................................
p44             GLLGELTSSEVATEVPFRLMHPQPEDPDTAKESA.................................................
BtArr3          GILGDLTASEVGVELPLILMHPKPSNEAAS.............................................SEDIVI
PmArr1          PLVG.....DLVAELPFTLMHPKPEEEPEVNN....KPAVPPASSPTQDPNSAPAVDTNLIELDTDGTTCYADQDDDIIF
BtArr1          GLLGDLASSDVAVELPFTLMHPKPKEEPP................HREVPEHETPVDTNLIELDTN........DDDIVF
HsArr1          GLLGDLASSDVAVELPFTLMHPKPKEEPP................HREVPENETPVDTNLIELDTN........DDDIVF
BtArr2          G........DVSVELPFVLMHPKPHDHIALPRPQS.APTHPPTLLPSAVPETDAPVDTNLIEFETNY.....ATDDDIVF
HsArr2          G........DVSVELPFVLMHPKPHDHIPLPRPQS.A...........APETDVPVDTNLIEFDTNY.....ATDDDIVF
AtVPS26like     SKLA................KAQPKSDPTAPRLWMALERLPLELV...........................RTKRDQFS
AtVPS26A        ED.....................RRYFKQQEITLYRLKEETS.................................
AtVPS26B        ED.....................RRYFKQQEITLYRLKEDASS................................
HsVPS26A        ED.....................RRYFKQQEIILWRKAPEKLR...............................KQRTNFH
BtVPS26A        ED.....................RRYFKQQEIILWRKAPEKLR...............................KQRTNFH
HsVPS26B        EE.....................RRYFKQQEVVLWRKGDIVRKSM............................SHQAAIAS
BtVPS26B        EE.....................RRYFKQQEVVLWRKGDIVRKSM............................SHQAAIAS

DpArr1          ..................................
p44             ..................................
BtArr3          EEFAQQEPSGESQ..EALAAEGNEGS......
PmArr1          EDFARLRLKGETE..A................
BtArr1          EDFARQRLKGMKD..DKEEEEDGTGSPRLNDR
HsArr1          EDFARQRLKGMKD..DKEEEEDGTGSPQLNNR
BtArr2          EDFARLRLKGLKD..EDYDDQFC.........
HsArr2          EDFARLRLKGMKD..DDYDDQLC.........
AtVPS26like     C.................................
AtVPS26A        ..................................
AtVPS26B        ..................................
HsVPS26A        QRFESPESQASAEQPEM................
BtVPS26A        QRFESPESQASAEQPEM................
HsVPS26B        QRFEGTTSLGEVRTPSQLSDNNCRQ.......
BtVPS26B        QRFEGTTPLGEARTPGPLSDSGNRQ.......
```

B.

1: DpArr1	100.00	37.22	38.42	46.98	46.61	46.89	43.13	42.03	19.03	18.22	19.77	15.44	15.44	16.73	16.73
2: p44		100.00	52.79	49.72	59.50	59.22	56.46	56.01	18.56	15.16	15.16	12.65	12.65	12.24	12.65
3: BtArr3			100.00	50.00	60.77	60.51	56.58	54.79	17.10	16.03	16.03	13.51	13.51	14.61	16.10
4: PmArr1				100.00	66.33	66.58	63.48	63.09	17.86	17.41	18.55	12.96	12.96	14.65	15.02
5: BtArr1					100.00	99.04	77.81	78.33	17.54	19.83	19.83	14.67	14.67	15.36	16.10
6: HsArr1						100.00	78.05	78.59	17.16	19.41	20.25	14.29	14.29	14.98	15.73
7: BtArr2							100.00	96.95	17.02	14.11	14.86	12.50	12.50	13.88	14.23
8: HsArr2								100.00	16.79	13.91	14.35	11.51	11.51	13.90	14.29
9: AtVPS26like									100.00	21.61	19.71	21.35	21.35	20.42	20.07
10: AtVPS26A										100.00	91.06	56.48	56.15	54.18	53.51
11: AtVPS26B											100.00	57.95	57.62	55.00	54.33
12: HsVPS26A												100.00	99.69	70.46	68.92
13: BtVPS26A													100.00	70.15	68.62
14: HsVPS26B														100.00	95.54
15: BtVPS26B															100.00

C.

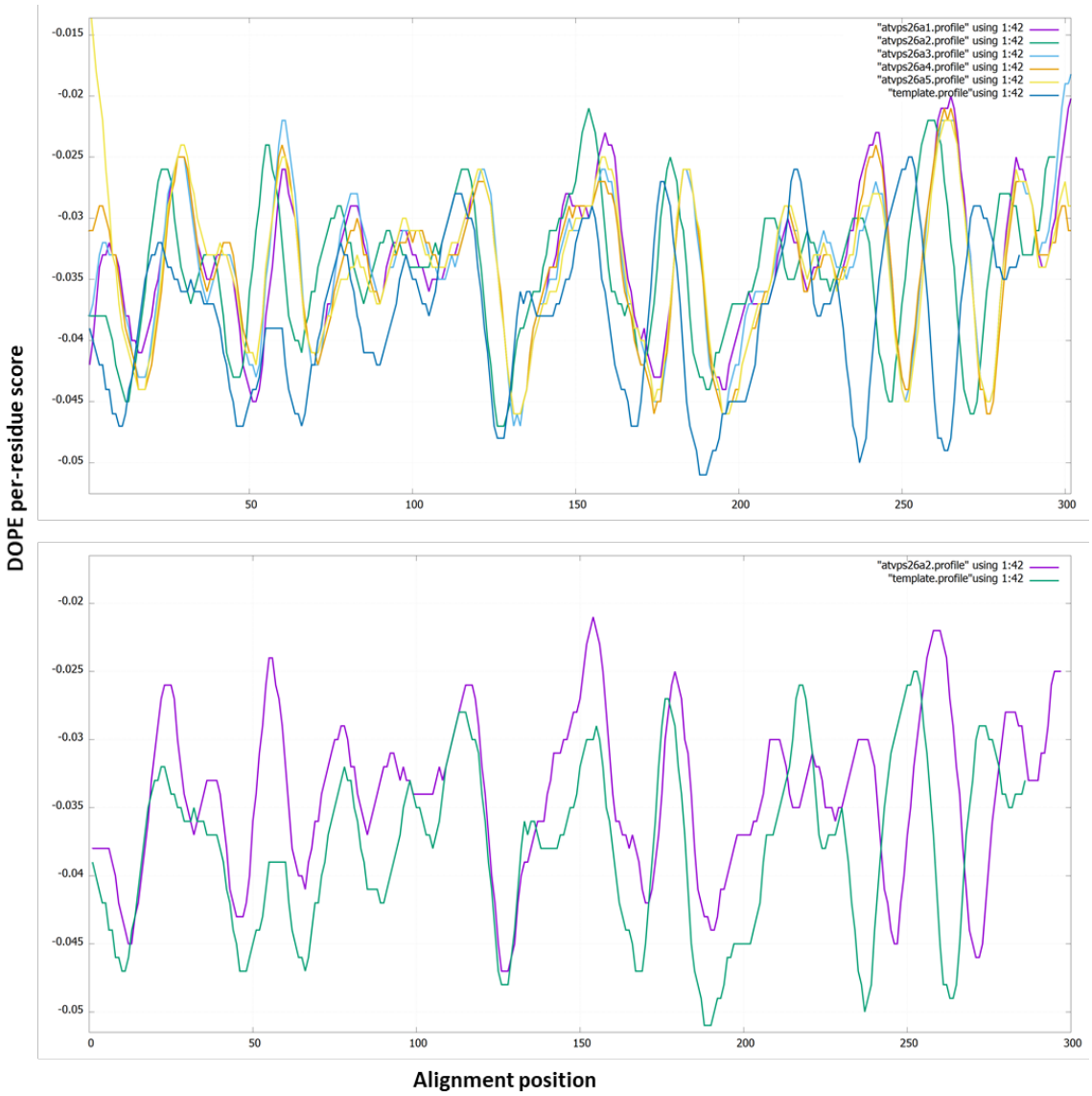
"atvps26a1.profile" using 1:42
"atvps26a2.profile" using 1:42
"atvps26a3.profile" using 1:42
"atvps26a4.profile" using 1:42
"atvps26a5.profile" using 1:42
"template.profile"using 1:42
-0.015
-0.02
-0.025
-0.03
-0.035
-0.04
-0.045
-0.05
50
100
150
200
250
300
"atvps26a2.profile" using 1:42
"template.profile"using 1:42
-0.02
-0.025
-0.03
-0.035
-0.04
-0.045
-0.05
0
50
100
150
200
250
300
DOPE per-residue score
Alignment position

1768 D.

Filename	molpdf	DOPE score	GA341 score	RMSD
atvps26a1.pdb	2292.41699	-30278.39648	1.00000	0.309
atvps26a2.pdb	2233.81055	-30840.71289	1.00000	0.17
atvps26a3.pdb	2258.48999	-30400.76953	1.00000	0.277
atvps26a4.pdb	2212.42798	-30568.29883	1.00000	0.244
atvps26a5.pdb	2188.86987	-30466.78711	1.00000	0.217

1769

1770 E.

1771

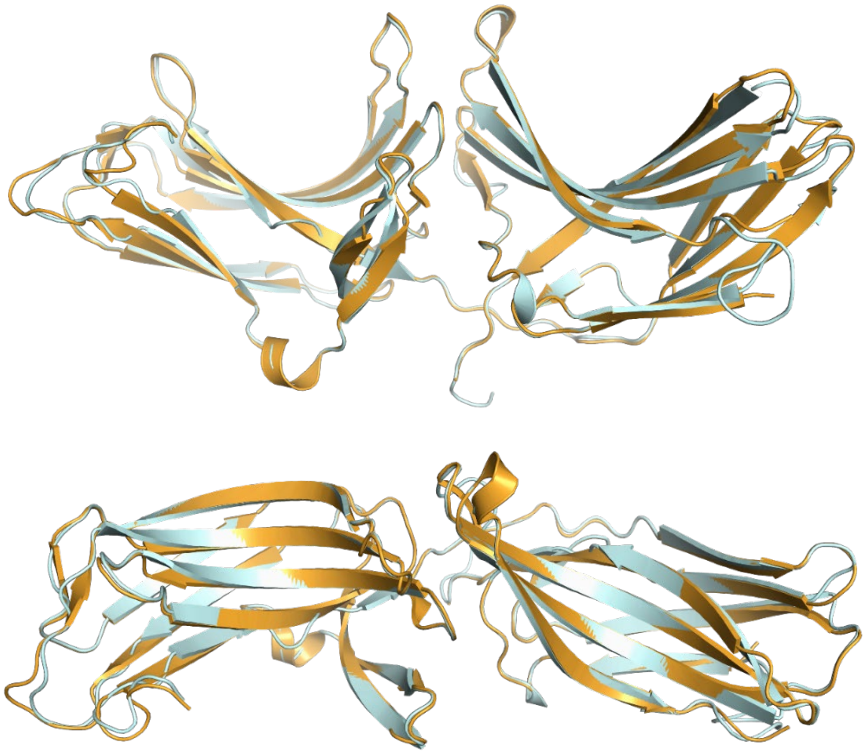

1772

1773

1774 **F.**

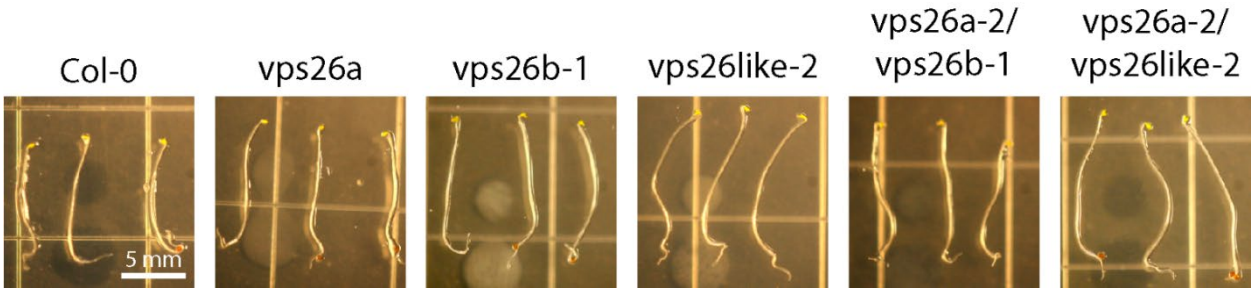

1775

Figure S5

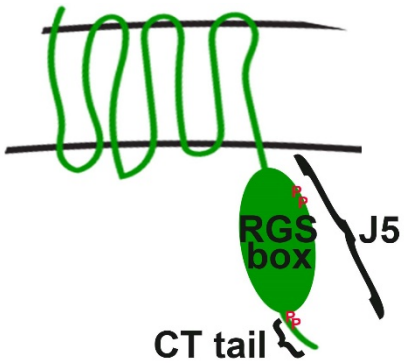

Figure S6

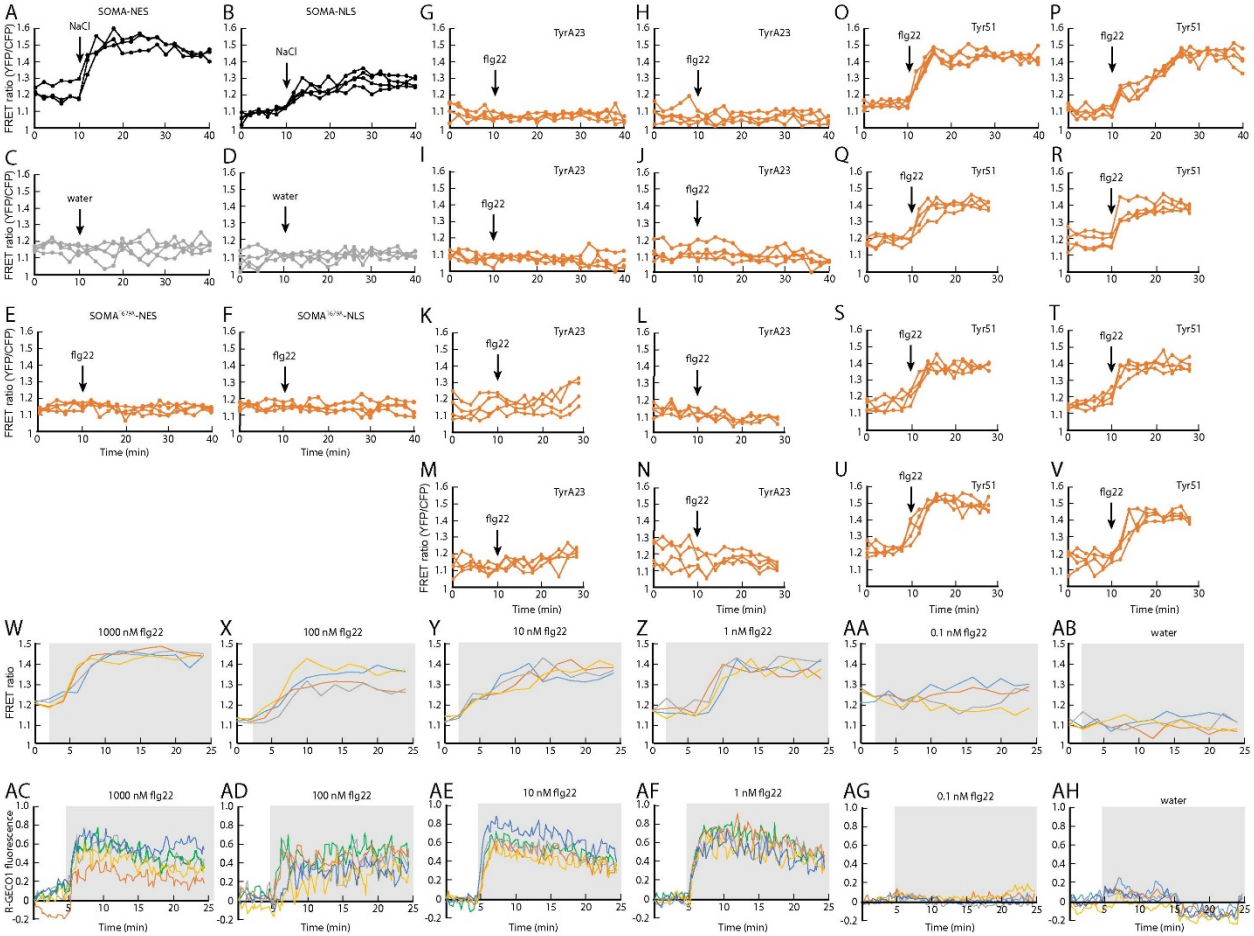

Supplemental code.

```
Data = xlsread('IMARIS statistics output’)
% first step: sort the data based on the track ID, and
% subsort it on time points.
sortedData=sortrows(Data,[3,4]);
trackIDs=sortedData(:,3);
%trackIDs is only the ith column from the original sorted data, separate
%array
uniquetrackIDs=unique(trackIDs);
%uniquetrackIDs is a separate array with only unique track IDs

%StartEnd=zeros(length(uniquetrackIDs),2);
meanSpeedArea=zeros(length(uniquetrackIDs),2);

% Make a matrix with all its elements zeros. One dimension of the matrix
% is length of unique track IDs, i.e., the number of unique track IDs.
% Another dimension is 2 because we want to store the start and end
% locations of each of the unique track IDs.
for i = 1:length(uniquetrackIDs)
    ItrackID=uniquetrackIDs(i);
    locations=find(trackIDs==ItrackID);
    startLoc=locations(1);
    endLoc=locations(end);
    SpeedColumn=sortedData(:,1);
    meanSpeedArea(i,1)=mean(SpeedColumn(startLoc:endLoc));
    AreaColumn=sortedData(:,2);
    meanSpeedArea(i,2)=mean(AreaColumn(startLoc:endLoc));
    %StartEnd(i,1)=startLoc;
    %StartEnd(i,2)=endLoc;

end
```